J. Fluid Mech. (2000), *vol.* 423, *pp.* 71–125. Printed in the United Kingdom

The theory of three-dimensional hetons and vortex-dominated spreading in localized turbulent convection in a fast rotating stratified fluid

By VLADIMIR M. GRYANIK[1,2], TATIANA N. DORONINA[1,2], DIRK J. OLBERS[1] AND TORSTEN H. WARNCKE[1]

[1]Alfred-Wegener-Institute for Polar and Marine Research, Bussestr 24, 27570 Bremerhaven, Germany

[2]A. M. Oboukhov Institute of Atmospheric Physics, Russian Academy of Sciences, Pyzhevsky 3, 109017 Moscow, Russia

(Received 4 March 1998 and in revised form 20 June 2000)

The problem of lateral heat/buoyancy transport in localized turbulent convection dominated by rotation in continuously stratified fluids of finite depth is considered. We investigate the specific mechanism of the vortex-dominated lateral spreading of anomalous buoyancy created in localized convective regions owing to outward propagation of intense heton-like vortices (pairs of vortices of equal potential vorticity (PV) strength with opposite signs located at different depths), each carrying a portion of buoyancy anomaly. Assuming that the quasi-geostrophic form of the PV evolution equation can be used to analyse the spreading phenomenon at fast rotation, we develop an analytical theory for the dynamics of a population of three-dimensional hetons. We analyse in detail the structure and dynamics of a single three-dimensional heton, and the mutual interaction between two hetons and show that the vortices can be in confinement, splitting or reconnection regimes of motion depending on the initial distance between them and the ratio of the mixing-layer depth to the depth of fluid (local to bulk Rossby radii). Numerical experiments are made for ring-like populations of randomly distributed three-dimensional hetons. We found two basic types of evolution of the populations which are homogenizing confinement (all vortices are predominantly inside the localized region having highly correlated wavelike dynamics) and vortex-dominated spreading (vortices propagate out of the region of generation as individual hetons or heton clusters). For the vortex-dominated spreading, the mean radius of heton populations and its variance grow linearly with time. The law of spreading is quantified in terms of both internal (specific for vortex dynamics) and external (specific for convection) parameters. The spreading rate is proportional to the mean speed of propagation of individual hetons or heton clusters and therefore depends essentially on the strength of hetons and the ratio of local to bulk Rossby radii. A theoretical explanation for the spreading law is given in terms of the asymptotic dynamics of a single heton and within the frames of the kinetic equation derived for the distribution function of hetons in collisionless approximation. This spreading law gives an upper 'advective' bound for the superdiffusion of heat/buoyancy. A linear law of spreading implies that diffusion parameterizations of lateral buoyancy flux in non-eddy-resolving models are questionable, at least when the spreading is dominated by heton dynamics. We suggest a scaling for the 'advective' parameterization of the buoyancy flux, and quantify the

exchange coefficient in terms of the mean propagation speed of hetons. Finally, we discuss the perspectives of the heton theories in other problems of geophysical fluid dynamics.

1. Introduction

1.1. *Problem definition and motivation*

Turbulent rotating convection in homogeneous and stratified fluids influences, controls and even dominates many physical events in natural geophysical and technical industrial flows (Hopfinger & van Heijst 1993; Boubnov & Golitsyn 1995). Turbulent convection dominated by rotation is characterized by strong horizontal intermittency due to the self-organization of the flow into isolated coherent vortices and into populations of such vortices. These vortices are long-lived features which maintain their identity. Their vertical and horizontal structures may be different depending on external parameters and the geometrical configuration. A wide range of governing external parameters such as the depth of the water column, the rotation rate, the surface buoyancy flux, and the buoyancy frequency of the initial density stratification was covered in laboratory experiments by Dikarev (1983), Boubnov & Golitsyn (1986, 1990, 1995), Fernando, Chen & Boyer (1991), Helfrich & Battisti (1991), Maxworthy & Narimousa (1994), Brickman (1995), Ivey, Taylor & Coates (1995), Whitehead, Marshall & Hufford (1996), and Narimousa (1998). Both quasi-barotropic cyclonic vortices, see e.g. Boubnov & Golitsyn (1986, 1990), and baroclinic heton-like vortices, see e.g. Helfrich & Battisti (1991), were observed. A heton-like vortex can be loosely defined as a pair of baroclinic vortices of the same strength, but opposite signs, located at different depths (we will give a more precise definition in the text below). The complex internal structure of localized vortices in turbulent convection with rotation was also observed in numerical simulations by Jones & Marshall (1993), Klinger & Marshall (1995), Sander, Wolf-Gladrow & Olbers (1995), and Käse (1998) who exploited constant diffusivity models and by Raasch & Etling (1991, 1998), and Mironov *et al.* (2000) in large-eddy simulations (LES). In particular, Klinger & Marshall (1995) simulated both fully three-dimensional and quasi-two-dimensional heton-like vortex structures. The heton-like vortices become more pronounced at high rotation rates (Sander *et al.* 1995; Klinger & Marshall 1995) owing to the two-dimensionalization of the flows.

Laboratory experiments such as those of Helfrich & Battisti (1991), Ivey *et al.* (1995), Narimousa (1998), Boubnov & Rhines (1999, personal communication) and numerical experiments such as those of Jones & Marshall (1993), Sander *et al.* (1995), Raasch & Etling (1998) and Käse (1998) clearly show that the localized convective region breaks up into populations of quasi-two-dimensional heton-like vortices and that heton-like vortices dominate the lateral spreading of heat and mass from a localized convective region. A schematic illustration of the population of heton-like vortices associated with convection events in a continuously stratified rotating fluid of finite depth H and mixed to the depth $-h$ is shown in figure 1. The circular area on the left-hand side shows a part of a localized cooling region with constant buoyancy flux at the surface. The figure also shows the phenomenon of vortex-dominated lateral spreading of anomalous buoyancy created by localized convection. Two heton-like vortices are presented in detail. Each of them consists of two baroclinic localized vortices, positive (cyclonic) at the surface and negative

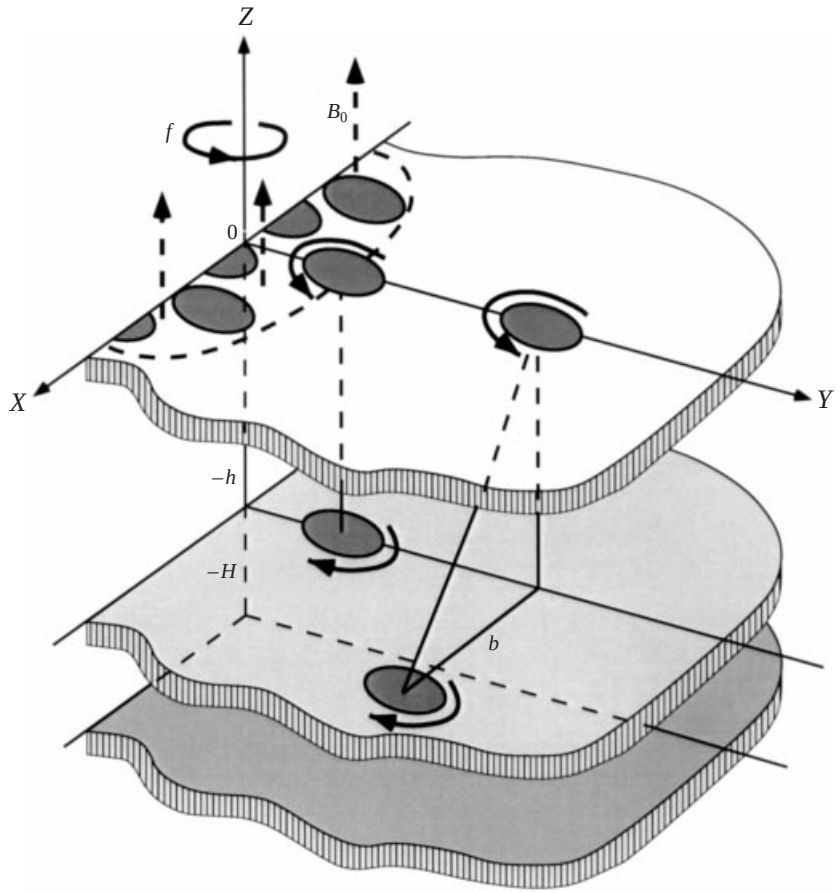

FIGURE 1. Schematic illustration of a three-dimensional heton population in a continuously stratified fluid, rotating with angular velocity f and of total depth H and mixing depth h. The circular area on the left-hand side shows a part of a localized cooling region, where B_0 is the constant buoyancy flux at the surface. Two hetons are shown in detail. Each of them consists of two baroclinic point vortices, positive (cyclonic) at the surface and negative (anticyclonic) at depth $-h$. At the instant of generation, a heton is aligned vertically (left heton). The right heton consists of two vortices which are not aligned. In the case presented here, the heton will propagate at a constant speed in the positive y-direction.

(anticyclonic) at the mixed-layer depth $-h$. Each baroclinic heton-like vortex appears as the result of the geostrophic adjustment of the geophysical fields generated by localized heat releases within the convection site and carries a buoyancy anomaly. At the instant of generation a heton-like vortex is aligned vertically (left heton). Owing to mutual interaction, heton-like vortices become tilted (right heton-like vortex in figure 1). Each tilted heton-like vortex possesses the property of self-propulsion (Gryanik 1983*a*, *b*). In the case presented here, the heton-like vortex propagates at some speed in the positive y-direction and transports a portion of the buoyancy anomaly out of the region of generation.

The phenomenon described above raises several questions about the physical mechanism of vortex-dominated lateral spreading of the buoyancy anomaly generated by localized convection in continuously stratified rotating fluids of finite depth:

(i) What is the characteristic structure of heton-like vortices when the mixing does not penetrate down to the bottom?

(ii) What are the characteristic dynamical regimes of motion for heton-like vortices? What are the necessary conditions for the spreading regime of motion to exist?

(iii) What is the law of the vortex-dominated spreading of the buoyancy anomaly? Is the spreading subdiffusive, diffusive, superdiffusive or 'advective'?

(iv) How can the structure, the regimes of motion and the spreading law be quantified in terms of internal parameters (related to vortex dynamics) and external parameters (related to convection)? In particular, how do they depend on the background stratification, the rotation rate, the depth of the fluid and the forcing?

(v) Is the law of vortex-dominated heat/buoyancy spreading consistent with the downgradient diffusion parameterizations of the buoyancy flux which are often used in non-eddy-resolving models? What is the scaling for the parameterization of the flux which takes into account the heat/buoyancy transport due to heton-like vortices?

When answering these questions we are primarily interested in understanding the fundamental dynamical processes, rather than in explaining the full complexity of oceanic and atmospheric flows with realistic equations of state. So, we consider idealized horizontally homogeneous incompressible fluids of infinite horizontal extent confined between two rigid horizontal boundaries. Moreover, we assume a uniform background stratification, a constant axisymmetric forcing, and a zero background flow, which are typical conditions used in recent laboratory experiments on localized convection in stratified fluids (see Ivey *et al.* 1995; Narimousa 1998). An insight into full complexity deep-ocean convection events can be gained in the review on observations and theories of Marshall & Schott (1999) about open-ocean deep-water formation in the Gulf of Lion, the central Labrador Sea, and the Greenland Sea. Our hope is that the understanding of the basis of lateral buoyancy transport gained from our work will apply to more complex situations, and other problems of geophysical fluid dynamics characterized by quasi-geostrophic vortex dominated spreading processes (some of them are mentioned in §§ 13 and 14). The knowledge of the mechanism of lateral spreading through the analysis of the spreading law can be helpful for the development of physically grounded parameterizations of the eddy heat/buoyancy transport in general circulation ocean models which are unable to resolve open-ocean deep-convection events. In particular, our results will show that the mean radius of a heton population and its variance grow linearly at large time. A linear law of heat/buoyancy spreading implies that downgradient diffusion parameterizations of lateral buoyancy transport commonly used to describe the spreading stage of deep ocean convection in non-eddy-resolving models (see e.g. discussion in Visbeck *et al.* 1997) are questionable, at least under conditions when the spreading is dominated by the dynamics of heton-like vortices.

1.2. *Approach and method*

The linear instability theory (see e.g. Pedlosky 1979; Boubnov & Golitsyn 1995) cannot be used to analyse the spreading events, because it describes only the short initial phase of a buoyancy anomaly development. The analytical nonlinear theory of Goncharov & Gryanik (1986), proposed for the treatment of the nonlinear vortex dynamics in laboratory experiments performed by Boubnov & Golitsyn (1986, 1990), can also not be applied to the analysis of a lateral spreading process, because this theory relies on the assumption that vortices have a quasi-barotropic cyclonic-like structure. The answers to the questions of the previous subsection can be given using

the dynamic theory of heton-like vortices in frames of the quasi-geostrophic (QG) approximation. The QG theory uses the property of two-dimensionalization of a flow at high rotation rate (Pedlosky 1979), focuses on the horizontal fluxes of buoyancy and emphasizes the transport due to localized vortices. The theory of heton-like vortices was developed in QG approximation starting from the works of Gryanik (1983*a*, *b*), where heton-like vortices were quantified as exact solutions of the QG potential vorticity (PV) evolution equation in point-vortex approximation, and the fundamental property of self-propulsion of hetons was studied, (see also the review of Hopfinger & van Heijst 1993). A pair of baroclinic point vortices in a two-layer QG model located in different layers having the same potential vorticity strength, but opposite signs, was called a heton by Hogg & Stommel (1985*a*), to emphasize the second fundamental property of hetons to transport heat. The term baroclinic vortex pair, has been used by Gryanik (1983*a*) for a two-layer model with layers of different thickness and a free surface, and by Gryanik (1983*b*) for a semi-infinite continuously stratified fluid. We should stress that the term heton can be used only in the case when the horizontal separations between vortices forming the heton are smaller than the barotropic Rossby radius (this ensures the applicability of the rigid-lid upper-boundary condition and the incompressibility of the fluid) which is always the case for the ocean as well as for laboratory experiments. At larger separations (typical for the atmospheres of Earth and giant planets), the effect of the barotropic Rossby radius simulates the compressibility of the atmosphere and should be taken into account. A baroclinic vortex pair in the latter case transports anomalies of internal thermobaric energy (see e.g. Gryanik 1983*a*), so, strictly speaking, the term heton cannot be used. Hogg & Stommel (1985*a*) analysed the basic regimes of interaction between point hetons in the two-layer model and used the theory (Hogg & Stommel 1985*b*) to study the conceptual physics of the spreading of warm pools of fluid on the Earth. Laboratory experiments with two-layer fluids demonstrated the efficiency and, at the same time, the limitations of the theoretical concept of point hetons, (see Griffiths & Hopfinger 1986; Hopfinger & van Heijst 1993). Using a two-layer QG model the stability of a single finite-core heton was analysed by Pedlosky (1985) and Kozlov, Makarov & Sokolovskiy (1986), the scattering of two finite-core hetons was studied by Sokolovskiy (1989), and Sokolovskiy & Verron (2000), the merging regime of interaction of finite-core hetons was investigated by Griffiths & Hopfinger (1986), Verron & Valcke (1996), and Sokolovskiy & Verron (2000). Legg & Marshall (1993) have developed a two-layer point heton model to include heat sources and used it to explore the equilibration of a circular convective region (a chimney in the ocean), see also Legg, Jones & Visbeck (1996) and Marshall & Schott (1999). Danilov, Gryanik & Olbers (2000) give a generalization of the two-layer model to the case of non-equal layer thickness to explore both the equilibration and spreading law of strip-shaped convective regions. The two-layer models cannot be applied directly to the case of a continuously stratified rotating fluid if the convective mixing does not penetrate down to the bottom. At least multi-layer versions of these models, similar to that considered by Gryanik & Tevs (1989, 1997), are required in this case. Multi-layer models, however, suppose that the PV anomaly associated with the heat release in localized convection has a piecewise continuous vertical structure, which is not always an appropriate approximation (see Pedlosky (1979) for a detailed comparison of multi-layer and continuously stratified QG models).

Progress in understanding the vortex-dominated lateral spreading of buoyancy anomalies in continuously stratified rotating fluids of finite depth can be achieved by generalizing the theory of QG three-dimensional baroclinic point vortices in semi-

infinite fluids (e.g. Charney 1963; Gryanik 1983*b*) to the theory of hetons in fluids of finite depth from one side, and by generalizing the heton theory of two-layer fluids (Gryanik 1983*a*; Hogg & Stommel 1985*a*) to the theory of hetons in continuously stratified fluids from the other.

Thus, assuming that the heat release associated with convection is intermittent horizontally within the cooled region and is homogeneous vertically within the mixed layer, we show that the baroclinic flow may be represented by populations of three-dimensional hetons, i.e. highly idealized QG PV distributions, which consist of a positive PV anomaly at the surface and a negative at the mixed-layer bottom having the same PV strength but of opposite sign. We adopt the term three-dimensional heton for the case of continuously stratified fluids here. Using this three-dimensional heton idealization and the PV evolution equation to compute the lateral spreading of buoyancy anomalies we will address the questions of § 1.1.

We stress that the QG approximation (Pedlosky 1979), which is the basic assumption of our theory and the numerical experiments, focuses the study only on the mechanism of lateral vortex-dominated spreading. The differences between simulations based on QG heton models and simulations based on LES models given by Raasch & Etling (1991, 1998) and Mironov *et al.* (2000), as well as constant-eddy diffusivity models performed by Jones & Marshall (1993) and Sander *et al.* (1995), can be accounted for in terms of two processes that QG heton models cannot resolve: ageostrophic generation of superinertial waves in the process of heton formation and evolution, and ageostrophic vertical mixing. The ageostrophic effect of the generation of superinertial waves from localized convective regions was investigated by Hermann & Owens (1993). They have shown that the energy loss by radiative processes is of the same order as that by advective hetons only for very narrow (a few Rossby radii) regions. The ageostrophic vertical-mixing processes were analysed in non-hydrostatic one- and two-dimensional mixed-layer models which are complementary to heton models, see e.g. the recent study of Straneo & Kawase (1999). However, in LES experiments and non-hydrostatic mixed-layer model experiments, the law of lateral spreading was not quantified, owing to the interaction of vortices with the periodic boundaries of the domain of integration in LES runs (Raasch 1999, personal communication), and owing to the inability of mixed-layer models to resolve baroclinic vortices. Moreover, so far we have not found in the literature experimental data quantifying the spreading law for localized convection regions in a continuously stratified rotating fluid, also due to the interaction of vortices with the boundaries of the rotating tank and dissipation in longtime experiments (Boubnov 1999, personal communication). However, in both numerical and laboratory experiments, the phenomenon of buoyancy spreading due to localized baroclinic vortices is clearly observed.

The paper is organized as follows. In § 2, we introduce the basic equations, present the concept of three-dimensional hetons and discuss the constraints on heton dynamics. In § 3, we specify the basic differential equations governing general point-vortex dynamics for the case of three-dimensional hetons. In § 4, the model is discussed in more detail for the case of uniform stratification (constant Brunt–Väisälä frequency). The basic cases of a vertically aligned and a tilted heton are considered in § 5. The interaction between two hetons is analysed in § 6. In § 7, the theory of lateral spreading is given in terms of the asymptotic dynamics of a single heton and within the frames of the kinetic equation derived for the distribution function of hetons in collisionless approximation. Numerical simulations with ring-like distributions of hetons intended to investigate the spreading law of heton populations, and a discussion of the results are presented in §§ 8 to 10. We formulate and analyse the spreading law in terms of

external parameters for the spreading of a chimney in the ocean in § 11. We consider the problem of the parameterization of eddy-heat transport in § 12. We discuss our results and propose problems for further study in § 13. Finally, we formulate the conclusions in § 14. In Appendices A to D, some analytical calculations which are of importance are presented.

2. Statement of the problem

As we have mentioned in § 1, the available laboratory and numerical experiments point out that baroclinic vortex structures formed during convection are long-lived formations preserving their shape for time intervals much larger than the geostrophic adjustment time. Hence, their dynamics at large time can be considered in the framework of quasi-geostrophic approximation. The quasi-geostrophic description is fully determined by specifying the distribution of the QG PV and its sources.

In a continuously stratified fluid, geostrophically adjusted flows are described by the well-known equation of potential vorticity evolution (e.g. Pedlosky 1979)

$$\frac{\partial Q}{\partial t} + (\Psi, Q) = S, \tag{2.1}$$

$$Q = \Delta\Psi + \frac{\partial}{\partial z}\left(\frac{f^2}{N^2}\frac{\partial \Psi}{\partial z}\right) \equiv \widehat{\mathscr{L}}\Psi, \tag{2.2}$$

where Ψ is the stream function, Q the quasi-geostrophic PV, f the Coriolis parameter and N the Brunt–Väisälä frequency. The Jacobian operator is defined as

$$(\Psi, Q) = \frac{\partial \Psi}{\partial x}\frac{\partial Q}{\partial y} - \frac{\partial Q}{\partial x}\frac{\partial \Psi}{\partial y}, \tag{2.3}$$

and the internal PV forcing is given by

$$S = \frac{\partial}{\partial z}\left(\frac{f}{N^2}\mathscr{B}\right), \tag{2.4}$$

where

$$\mathscr{B} = \frac{g\alpha\mathscr{Q}}{c_p\rho_0} \tag{2.5}$$

is the buoyancy release rate. Here, g is the acceleration due to gravity, α the thermal expansion coefficient, c_p the specific heat at constant pressure, ρ_0 the reference density and $\mathscr{Q}$ the heat release rate per unit volume.

The horizontal velocity $\boldsymbol{u} = (u, v)$, the vertical velocity w, the pressure p and the density ρ or buoyancy η are then given by

$$u = -\frac{\partial \Psi}{\partial y}, \quad v = \frac{\partial \Psi}{\partial x}, \tag{2.6}$$

$$w = -\frac{f}{N^2}\left(\frac{\partial}{\partial t}\frac{\partial \Psi}{\partial z} + \left(\Psi, \frac{\partial \Psi}{\partial z}\right)\right) + \frac{\mathscr{B}}{N^2}, \tag{2.7}$$

$$p = f\rho_0\Psi, \tag{2.8}$$

$$\rho = -\frac{\rho_0}{g}\eta = -\frac{f\rho_0}{g}\frac{\partial \Psi}{\partial z}. \tag{2.9}$$

The rigid-lid boundary conditions are

$$w = 0 \quad \text{for } z = 0, \quad z = -H. \tag{2.10}$$

In a continuously stratified and rotating fluid, convective mixing in the form of plumes penetrates down to depth z_i. Correspondingly, the heat forcing $\mathscr{Q}$, which represents the resulting effect of unresolved convective motions that distribute the cooling induced by heat loss at the surface, exists also only within this region. We choose a buoyancy forcing function $\mathscr{B}$, see equation (2.5), of the form

$$\mathscr{B} = \overline{\mathscr{B}}\,\mathscr{R}(x, y) \times \mathscr{Z}(z) \times \mathscr{T}(t), \tag{2.11}$$

where the functions $\mathscr{R}(x, y)$ and $\mathscr{Z}(z)$ specify the horizontal and vertical forcing distribution, $\mathscr{T}(t)$ their temporal behaviour, and $\overline{\mathscr{B}}$ represents the magnitude.

Consider the case of the localized horizontal distribution source of

$$\mathscr{R}(x, y) = \mathscr{A}_0\,\delta(x - x_0)\,\delta(y - y_0), \tag{2.12}$$

where (x_0, y_0) is the position of the source and $\mathscr{A}_0$ is a characteristic area. This source represents the integral effect of the heat release by the rotation-dominated plumes at times larger than the geostrophic adjustment time. This is in agreement with results of laboratory experiments (Boubnov & Golitsyn 1986; Ivey *et al.* 1995) and high-resolution numerical LES experiments (Raasch & Etling 1998; Mironov *et al.* 2000) with heat forcing, which show strong horizontal intermittency of a temperature field. The intermittency is much less pronounced in experiments with buoyancy forcing and in low-resolution numerical simulations based on the constant diffusivity models.

The vertical distribution is taken to be of the form

$$\mathscr{Z}(z) = \Theta(-z) - \Theta(z_0 - z), \tag{2.13}$$

where $\Theta(z)$ is the Heaviside step function. This representation is a consequence of the hypothesis that the heat source is homogeneously distributed with depth. The assumption of a homogeneous vertical heat distribution implies that the vertical heat flux decreases linearly with depth from the surface value to zero at the boundary of the mixing region. This is in agreement with results of numerical simulations with LES models by Raasch & Etling (1991, 1998) and Mironov *et al.* (2000). According to Raasch & Etling (1991), and Mironov *et al.* (2000), the vertical heat flux takes low positive values at the boundary of the mixing zone which could be explained by entrainment of colder non-turbulent fluid and wave motions due to the presence of internal gravity waves. These effects can be neglected in the framework of quasi-geostrophic approximation, i.e. on times that are greater than the time of geostrophic adaptation of the geophysical field to geostrophic and hydrostatic equilibrium.

Localized baroclinic vortex structures are formed during convection events at time intervals τ_0 (the vertical mixing timescale) which are much smaller than the geostrophic adjustment time and the timescale of quasi-geostrophic evolution. This makes it possible to specify the time dependence of the forcing by introducing the delta-function description

$$\mathscr{T}(t) = \tau_0\,\delta(t - t_0). \tag{2.14}$$

The solution of equation (2.1) for the source specified above is

$$Q = \gamma_0\,\Theta(t - t_0)\delta(x - x_0)\,\delta(y - y_0)\,[\delta(z) - \delta(z_0 - z)], \quad \gamma_0 = -\frac{f}{N^2}\overline{\mathscr{B}}\mathscr{A}_0\tau_0, \tag{2.15}$$

where γ_0 is the vortex strength. The horizontal vortex coordinates are (x_0, y_0) and coincide with the horizontal coordinates of the localized source. Each three-dimensional

heton has the deficit of buoyancy. A baroclinic vortex with such a vertical distribution of PV will be referred to further as a three-dimensional heton.

The simplified forcing profile (equations (2.12) and (2.13)) can be considered as a basic one. Any other profile (which vanishes at $z = 0$ and $z = z_i$) can be formed from it by convolution, or, in practice, approximated by a finite set of such profiles. Thus, under all assumptions mentioned above, we finally have a PV source

$$S = \sum_{i=1}^{\mathscr{N}} \gamma_i \, \delta(x - x_i) \, \delta(y - y_i) \, [\delta(z) - \delta(z_i - z)] \, \delta(t - t_i), \tag{2.16}$$

where γ_i is given by

$$\gamma_i = -\frac{f}{N^2} \overline{\mathscr{B}} \mathscr{A}_i \tau_i. \tag{2.17}$$

In principle all the forcing parameters γ_i, x_i, y_i, z_i and t_i in equation (2.16) could be prescribed as random variables with given statistics. A model of barotropic point vortices in which a prognostic equation for the intensity of the vortices was specified as a first-order Markov process, and where the initial conditions were prescribed, was considered by Egger (1992). A two-layer model of point-vortex hetons, in which the intensity of the hetons was constant, but initial coordinates were random with the additional constraint that newly created hetons must be at a distance larger than the Rossby radius from the existing hetons, was analysed by Legg & Marshall (1993).

If initially (that is before cooling) the fluid is at rest, then the total momentum and angular momentum of the emerging vortex structure should remain zero for all time. In our quasi-geostrophic approximation they are

$$\mathscr{P}_x = \rho_0 \int yQ \, \mathrm{d}x \, \mathrm{d}y \, \mathrm{d}z = 0, \quad \mathscr{P}_y = -\rho_0 \int xQ \, \mathrm{d}x \, \mathrm{d}y \, \mathrm{d}z = 0 \tag{2.18}$$

and

$$\mathscr{J} = \rho_0 \int \left(x^2 + y^2\right) Q \, \mathrm{d}x \, \mathrm{d}y \, \mathrm{d}z = 0, \tag{2.19}$$

respectively. For our heat source, i.e. our PV source (2.16), the intensities of vortices in each three-dimensional heton are equal by magnitude and have opposite signs, so that

$$\int Q \, \mathrm{d}x \, \mathrm{d}y \, \mathrm{d}z = 0, \tag{2.20}$$

and in agreement with constraints (2.18), (2.19) and (2.20) all vortices are aligned vertically at the instant of generation.

With all these idealizations, such a model distribution of buoyancy forcing allows us to investigate the structure and dynamics of baroclinic vortices as a function of the mixing depth z_i and the forcing parameters γ_i. In this respect, the model is minimal.

3. Basic three-dimensional heton model

We search for exact solutions Q of the quasi-geostrophic potential vorticity equation (2.1) with sources (2.16), having the following form:

$$Q = Q_0 + Q_v, \tag{3.1}$$

$$Q_v = \sum_{i=1}^{\mathscr{M}} \Gamma_i(t) \, \delta(x - x_i(t)) \, \delta(y - y_i(t)) \, \delta(z - z_i(t)), \tag{3.2}$$

where Q_0 is the potential vorticity of the background flow and Q_v is that of the point vortices where $x_i(t)$, $y_i(t)$, $z_i(t)$ are the vortex coordinates. The index i passes through all $\mathscr{M} = 2\mathscr{N}$ vortices.

The stream function of the background flow is Ψ_0 and the stream function of the flow associated with the point vortices is

$$\Psi_v(x, y, z) = \sum_{i=1}^{\mathscr{M}} \Gamma_i(t)\, G(x, y, z;\ x_i(t), y_i(t), z_i(t)). \tag{3.3}$$

Here, G is Green's function defined in the usual way

$$\widehat{\mathscr{L}} G(x, y, z;\ x_0, y_0, z_0) = \delta(x - x_0)\,\delta(y - y_0)\,\delta(z - z_0), \tag{3.4}$$

with the boundary conditions

$$\partial_z G = 0 \quad \text{at } z = 0, -H. \tag{3.5}$$

Substituting equations (3.2) and (3.3) into equation (2.1) and equating the regular terms and the terms with the δ-functions and their derivatives, we obtain the following system of ordinary differential equations that define the evolution of the regular background flow and the geostrophic point vortices:

$$\frac{\mathrm{d}\Gamma_i}{\mathrm{d}t} = \Gamma_i\,\delta(t - t_i), \tag{3.6}$$

$$\frac{\mathrm{d}z_i}{\mathrm{d}t} = 0, \tag{3.7}$$

$$\frac{\mathrm{d}x_i}{\mathrm{d}t} = -\sum_{j=1,\ j\neq i}^{\mathscr{M}} \Gamma_j \frac{\partial G}{\partial y}\bigg|_{r_i} - \frac{\partial \Psi_0}{\partial y}\bigg|_{r_i} \tag{3.8}$$

$$\frac{\mathrm{d}y_i}{\mathrm{d}t} = \sum_{j=1,\ j\neq i}^{\mathscr{M}} \Gamma_j \frac{\partial G}{\partial x}\bigg|_{r_i} + \frac{\partial \Psi_0}{\partial x}\bigg|_{r_i} \tag{3.9}$$

$$\frac{\partial Q_0}{\partial t} + (\Psi_0, Q_0) + \sum_{i=1}^{\mathscr{M}} \Gamma_i (G, Q_0) = 0, \tag{3.10}$$

with the additional conditions at $t = t_i$

$$\Gamma_{2i-1}(t_i) \equiv \gamma_{ci} = \gamma_i, \quad \Gamma_{2i}(t_i) \equiv \gamma_{ai} = -\gamma_i, \tag{3.11}$$

as well as

$$\left.\begin{aligned} &(x_{2i-1}(t_i), y_{2i-1}(t_i), z_{2i-1}(t_i)) \equiv (x_{ci}, y_{ci}, 0), \\ &(x_{2i}(t_i), y_{2i}(t_i), z_{2i}(t_i)) \equiv (x_{ai}, y_{ai}, z_{ai}). \end{aligned}\right\} \tag{3.12}$$

Here, the index c refers to cyclonic vortices and the index a to anticyclonic vortices, because $\gamma_i > 0$ for the case under consideration ($\mathscr{Q} < 0$).

Clearly, if all t_i are identical, the problem with the heat source, see (2.16), is equivalent to an initial-value problem for three-dimensional point vortices considered by Charney (1963) and Gryanik (1983*b*). In this case, according to equation (3.6), the vortex intensities remain unchanged with time. The system of equations (3.7), (3.8) and (3.9) shows that each geostrophic point vortex is transported at a velocity equal to the sum of that in the regular flow and that induced by all other vortices at the location of the considered geostrophic point vortex. Note, that the flow associated

with a vortex does not transport its own potential vorticity. Geostrophic point vortices in turn induce a transport of the regular vorticity distribution, as given by the last term in equation (3.10).

Using equations (3.6), (3.11) and (3.7), (3.12) we obviously have

$$\gamma_{ci}(t) = -\gamma_{ai}(t) = \gamma_i, \tag{3.13}$$

$$z_{ci}(t) = 0, \quad z_{ai}(t) = z_{ai}(0) = z_i. \tag{3.14}$$

Thus, an ensemble consisting of $\mathscr{M} = 2\mathscr{N}$ vortices forms $\mathscr{N}$ hetons during its entire evolution.

4. Specification of the model for the case of constant Brunt–Väisälä frequency and zero background flow

We consider further a horizontally homogeneous fluid of infinite horizontal extent confined between two rigid horizontal boundaries at $z = 0$ and $z = -H$ which in the absence of disturbances has a uniform stratification (Brunt–Väisälä frequency $N = \text{const}$). We set the background flow to zero, so $Q_0 = 0$. We assume that convective mixing penetrates down to the mixing depth $-h$, so we take

$$z_{ci} = 0, \quad z_{ai} = -h. \tag{4.1}$$

We also assume

$$\gamma_{ci} = \gamma, \quad \gamma_{ai} = -\gamma, \tag{4.2}$$

which is a consequence of the assumption about the vertical structure of the buoyancy flux. So we have a heton consisting of a pair of opposite-sign point vortices, a cyclonic one at the surface $z = 0$ with strength $\gamma > 0$, and an anticyclonic one at $z = -h$ with strength $-\gamma < 0$.

4.1. *Green's function*

Green's function $G(r, z, z_0)$ describes the flow induced by an individual baroclinic point vortex of unit strength having the coordinates $(0, 0, z_0)$. In the case of a homogeneously stratified fluid between two horizontal boundaries it is given by

$$G(r, z, z_0) = \sum_{m=-\infty}^{+\infty} \{G_0(r, z - z_0 + 2Hm) + G_0(r, z + z_0 + 2Hm)\}, \tag{4.3}$$

where

$$G_0(r, z) = -\frac{N}{4\pi f}\left(r^2 + \frac{N^2}{f^2}z^2\right)^{-1/2} \tag{4.4}$$

is Green's function in an unbounded fluid. In our notation $G(x, y, z;\ x_0, y_0, z_0) = G(r, z, z_0)$ where $r = \left((x - x_0)^2 + (y - y_0)^2\right)^{1/2}$.

Green's function can be written in another form (see Appendix A for details):

$$G(r, z, z_0) = \frac{1}{H}\left[g_0(r) + 2\sum_{n=1}^{\infty} g_n(r) Z_n(z) Z_n(z_0)\right], \tag{4.5}$$

where the horizontal part is

$$g_n(r) = \begin{cases} \dfrac{1}{2\pi}\ln\left(\dfrac{re^c}{2L_0}\right), & n = 0 \\ -\dfrac{1}{2\pi}K_0(\lambda_n r), & n = 1, 2, \ldots, \end{cases} \tag{4.6}$$

with $\lambda_n = \pi n/L$, $L = NH/f$ the bulk Rossby radius, L_0 the barotropic Rossby radius, $K_0(r)$ the modified Bessel function, c Euler's constant and

$$Z_0 = 1, \quad Z_n = \cos\left(\frac{\pi n}{H}z\right). \tag{4.7}$$

4.2. *Scaling and governing equations*

Throughout the next part of this paper all variables will be considered non-dimensional unless otherwise specified. We set the horizontal scale L equal to the bulk Rossby radius and the vertical scale l equal to the ocean depth:

$$L = \frac{N}{f}H, \quad l = H. \tag{4.8}$$

For the timescale we choose

$$T = \frac{L^3}{\gamma(N/4\pi f)} = \left(\frac{N}{f}\right)^2 \frac{4\pi H^3}{\gamma} \tag{4.9}$$

in order to simplify the following dynamical equations. The scaling implies a Rossby number

$$Ro = \frac{1}{Tf} = \left(\frac{f}{N}\right)^2 \frac{\gamma}{4\pi f H^3}. \tag{4.10}$$

The population of three-dimensional hetons is then characterized by the geometrical non-dimensional parameters

$$d = \frac{h}{H}, \quad R_{hor} = \frac{L_{hor}}{L}, \tag{4.11}$$

where L_{hor} is the characteristic horizontal scale of the heton distribution which depends upon the problem under consideration and will be specified later.

The presence of the non-dimensional parameter d implies that there exists another, local, Rossby radius

$$L_h = \frac{N}{f}h = Ld. \tag{4.12}$$

As will be shown later, this parameter is the main scale determining the nonlinear interactions between hetons and thus their dynamics.

In non-dimensional variables the equations of motion are

$$\frac{\mathrm{d}x_{ci}}{\mathrm{d}t} = -\sum_{j=1,\ j\neq i}^{\mathcal{N}} \frac{\partial}{\partial y_{ci}} G(r_{ci,cj}, 0, 0) + \sum_{j=1}^{\mathcal{N}} \frac{\partial}{\partial y_{ci}} G(r_{ci,aj}, 0, -d), \tag{4.13}$$

$$\frac{\mathrm{d}y_{ci}}{\mathrm{d}t} = \sum_{j=1,\ j\neq i}^{\mathcal{N}} \frac{\partial}{\partial x_{ci}} G(r_{ci,cj}, 0, 0) - \sum_{j=1}^{\mathcal{N}} \frac{\partial}{\partial x_{ci}} G(r_{ci,aj}, 0, -d), \tag{4.14}$$

$$\frac{\mathrm{d}x_{ai}}{\mathrm{d}t} = -\sum_{j=1,\ j\neq i}^{\mathscr{N}} \frac{\partial}{\partial y_{ai}} G(r_{ai,aj}, -d, -d) + \sum_{j=1}^{\mathscr{N}} \frac{\partial}{\partial y_{ai}} G(r_{ai,cj}, -d, 0), \tag{4.15}$$

$$\frac{\mathrm{d}y_{ai}}{\mathrm{d}t} = \sum_{j=1,\ j\neq i}^{\mathscr{N}} \frac{\partial}{\partial x_{ai}} G(r_{ai,aj}, -d, -d) - \sum_{j=1}^{\mathscr{N}} \frac{\partial}{\partial x_{ai}} G(r_{ai,cj}, -d, 0). \tag{4.16}$$

Here, $r_{ci,cj} = \left((x_{ci} - x_{cj})^2 + (y_{ci} - y_{cj})^2\right)^{1/2}$ is the distance between two cyclonic vortices in the horizontal plane. Corresponding expressions are introduced for distances between anticyclonic vortices and for distances between cyclonic and anticyclonic vortices.

4.3. *Hamiltonian description and integrals of motion*

For the case under consideration the system of equations (4.13)–(4.16) is Hamiltonian for each time interval $t_i < t < t_{i+1}$, see Appendix B:

$$\frac{\mathrm{d}x_i}{\mathrm{d}t} = \frac{\partial \mathscr{H}}{\partial y_i}, \qquad \frac{\mathrm{d}y_i}{\mathrm{d}t} = -\frac{\partial \mathscr{H}}{\partial x_i}, \tag{4.17}$$

the index i here refers to both cyclones and anticyclones. The Hamiltonian coincides with the energy

$$\mathscr{H} = -\sum_{\substack{i,j=1 \\ i<j}}^{\mathscr{N}} [G(r_{ci,cj}, 0, 0) + G(r_{ai,aj}, -d, -d)] + \sum_{i,j=1}^{\mathscr{N}} G(r_{ci,aj}, 0, -d) \tag{4.18}$$

of mutual interaction which does not depend explicitly on time, and thus is a constant of motion.

Furthermore, $\mathscr{H}$ is invariant to translation and rotation of x, y coordinates. Correspondingly, these symmetries imply the conservation laws of momentum and angular momentum. In our case, as was explained earlier, these integrals are equal to zero (see equations (2.18) and (2.19)), so

$$\mathscr{P}_x = \sum_{i=1}^{\mathscr{N}} (y_{ci} - y_{ai}) = 0, \qquad \mathscr{P}_y = -\sum_{i=1}^{\mathscr{N}} (x_{ci} - x_{ai}) = 0, \tag{4.19}$$

$$\mathscr{J} = \sum_{i=1}^{\mathscr{N}} \left[(x_{ci}^2 + y_{ci}^2) - (x_{ai}^2 + y_{ai}^2)\right] = 0. \tag{4.20}$$

Using these three integrals, a new integral may be introduced which corresponds to the conservation of relative angular momentum

$$\mathscr{I} = \sum_{i,j=1}^{\mathscr{N}} [(x_{ci} - x_{cj})^2 + (y_{ci} - y_{cj})^2 + (x_{ai} - x_{aj})^2 + (y_{ai} - y_{aj})^2 - 2[(x_{ci} - x_{aj})^2 - (y_{ci} - y_{aj})^2]] = 0. \tag{4.21}$$

This integral, as well as the Hamiltonian, depends only on relative positions of vortices and can be conveniently used in analysing relative heton motions.

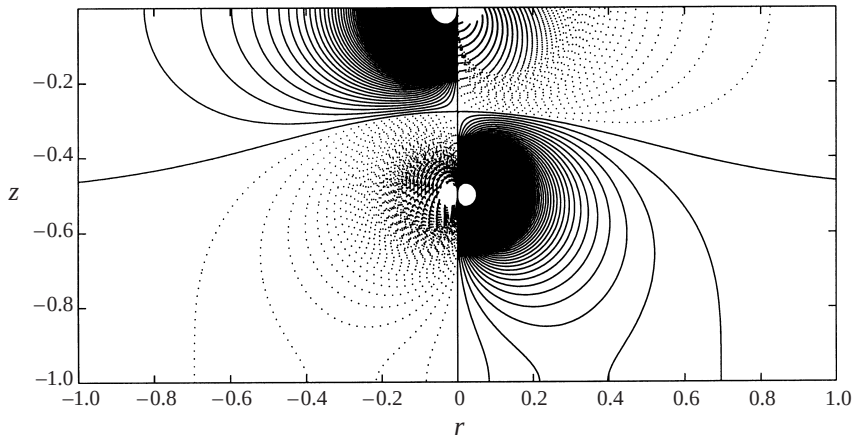

FIGURE 2. Vertical (x, z)-section of the azimuthal velocity induced by a single three-dimensional heton at the instant of generation (see left-hand heton in figure 1). The contours correspond to isolines of the velocity. The direction of the velocity is normal to the plane, where the dashed lines represent the ingoing and the solid lines the outcoming flow.

5. A single three-dimensional heton

As we can see, the simplest object in the theory is a single heton, see vertically aligned left-hand heton and the tilted right-hand heton in figure 1.

5.1. *Vertically aligned three-dimensional heton*

Let us consider a heton that at the instant of generation has coordinates $x_c = x_a = 0$, $y_c = y_a = 0$, $z_c = 0$ and $z_a = -d$. This vertically aligned three-dimensional heton has $\mathscr{P}_x = \mathscr{P}_y = 0$ and $\mathscr{J} = 0$, see equations (4.19) and (4.20), so it remains at rest all the time if it does not interact with other hetons.

The structure of the flow associated with a heton is described by the stream function:

$$\Psi = G(\sqrt{x^2 + y^2}, z, 0) - G(\sqrt{x^2 + y^2}, z, -d). \tag{5.1}$$

The heton structure is axisymmetric. As can be seen from (5.1) the heton has purely baroclinic structure due to cancellation of the barotropic parts of Green's function (4.5) in equation (5.1).

In the limit, $r \to \infty$, that is for r much greater than the bulk Rossby radius L ($L = 1$ in our units), equations (5.1), (4.5) and (4.6) show an exponential decay for all flow fields. This result follows from the exponential decay of the modified Bessel functions $K_n(r) \sim r^{-1/2}\exp(-r)$ for $r \gg 1$. Thus, the bulk Rossby radius L defines the maximum horizontal size of a heton field at the instant of its generation. In particular, the azimuthal velocity $u(r, z)$ is calculated by substituting equation (5.1) into (2.6). For $r \gg 1$, $u(r, z) \sim K_1(\lambda_1 r) \sim r^{-1/2}\exp(-\lambda_1 r)$. A sketch of the azimuthal velocity $u(x, z)$ is given in figure 2. The structure of the azimuthal velocity field shown in figure 2 has evident similarities with the structure of the heton field calculated in numerical experiments by Klinger & Marshall (1995), see their figure 2.

Each vertically aligned three-dimensional heton has the deficit $\mathscr{D}$ of buoyancy

$$\mathscr{D} = 2\pi \int \eta(r, z)\, r\, \mathrm{d}r\, \mathrm{d}z = \gamma \frac{N^2 h}{f}, \tag{5.2}$$

where buoyancy is given by (2.9). See derivation of (5.2) in Appendix C.

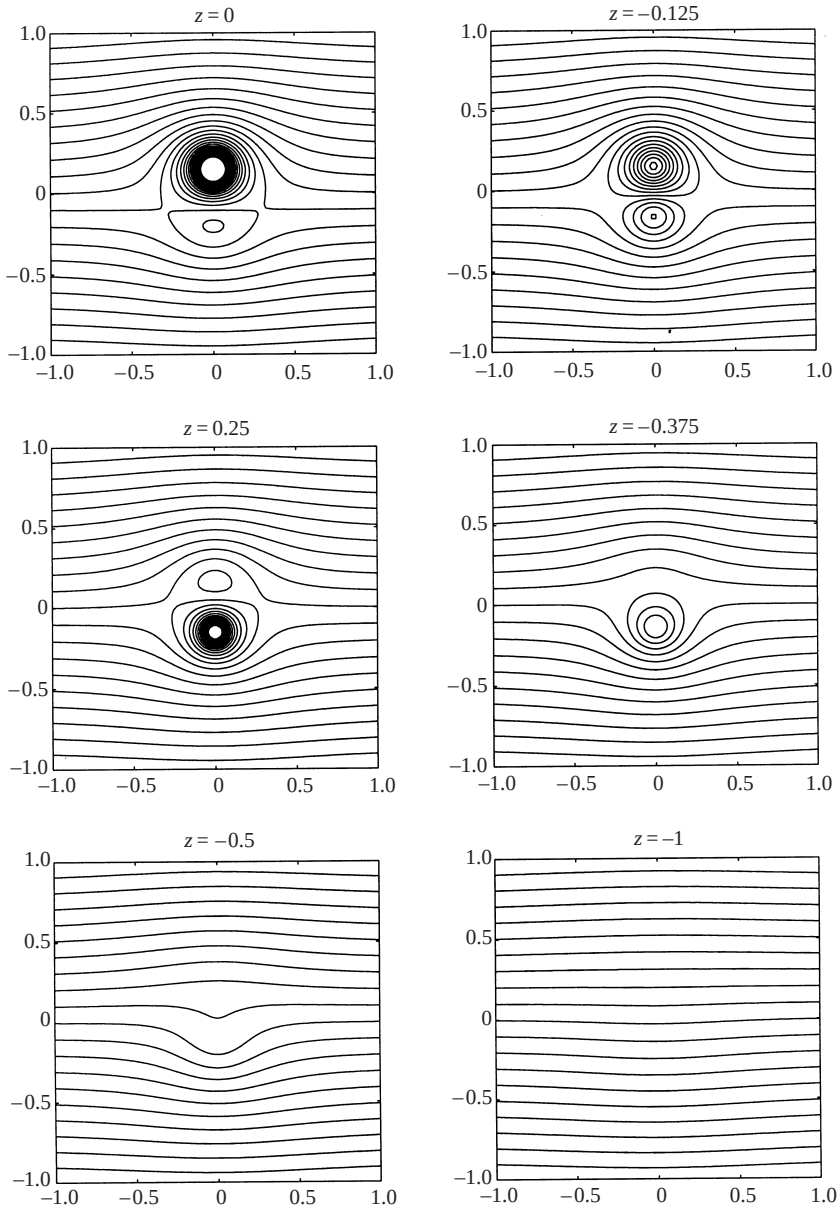

FIGURE 3. Sections at different depths z of the stream function of a single heton with parameters $a = 0$, $b = 0.3$ and $d = 0.25$. The stream function is represented in the reference frame translating with the heton.

5.2. *Tilted three-dimensional heton*

Suppose that we have $x_c = x_a = 0$ and $y_c = -y_a = b/2$. We will call such a heton a tilted heton. Tilted hetons naturally arise because of interaction between vertically aligned hetons, as will be shown in the next sections. A tilted three-dimensional heton has non-zero momentum $\mathscr{P}_x = 2b, \mathscr{P}_y = 0$, so there is the property of self-propagation.

The speed of a single tilted heton is the basic characteristic of its evolution. Let us

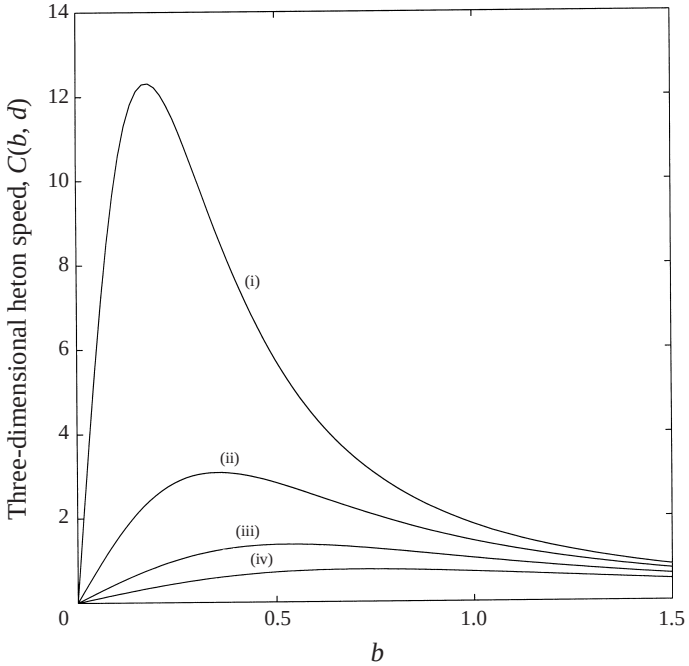

FIGURE 4. Speed of a single three-dimensional heton for different depths and separations: (i) $d = -0.25$; (ii) $d = -0.5$; (iii) $d = -0.75$; (iv) $d = -1.0$.

analyse it in detail. For $\mathcal{N} = 1$, (4.19) shows that the distance b, between cyclonic and anticyclonic vortices in the heton, remains constant and equations (4.13) to (4.16) have the solution:

$$x_c = x_a = Ct, \qquad y_c = -y_a = \tfrac{1}{2}b \tag{5.3}$$

describing a heton which translates at a constant speed C, where

$$C = -\frac{\partial}{\partial b}G(b, 0, -d). \tag{5.4}$$

Using (4.3) and (4.4) we obtain

$$C = \sum_{m=-\infty}^{+\infty} \frac{2b}{[b^2 + (d + 2m)^2]^{3/2}}. \tag{5.5}$$

This solution, describing the velocity function $C = C(b, d)$ for various height differences in the range $0 < d < 1$, is represented in figure 4 as a function of b. The function has a single maximum with a magnitude which decreases when d increases.

We consider several limiting cases. If $b^2 + d^2 \ll 1$, the solution (5.5) becomes

$$C = \frac{2b}{(b^2 + d^2)^{3/2}}. \tag{5.6}$$

This solution was obtained by Gryanik (1983*b*) for the case of a semi-infinite fluid domain, that is for $H \to \infty$. Here it corresponds to the limit of a small aspect ratio d.

For $b \ll d$, we have

$$C = b\left[\frac{2}{d^3} + \tfrac{1}{4}\zeta\left(3, \frac{d}{2}\right) + \tfrac{1}{4}\zeta\left(3, -\frac{d}{2}\right)\right], \tag{5.7}$$

where $\zeta(q, z)$ is Riemann's zeta function.

In the other limit, $b > \lambda_1^{-1}$, that is for the horizontal heton size greater than the bulk Rossby radius L ($L = 1$ in our units), the propagation speed can be estimated using the two first terms in (4.5) and (4.6). In this approximation (5.4) gives

$$C = \frac{2}{b}\left[1 + \lambda_1 b K_1(\lambda_1 b)\cos(\pi d)\right]. \tag{5.8}$$

Remarkably, for $d = 1$, the propagation speed given by (5.8) coincides with the propagation speed of a heton in a two-layer model of equal thickness (see Gryanik 1983*b*; Hogg & Stommel 1985*a*), when λ_1^{-1} is identified with the Rossby radius of the two-layer model and $2\gamma/H = \kappa$ is the strength of the heton in the two-layer model. The speed is independent of d for $b \gg 1$ owing to the barotropic nature of the flow at these distances. This speed coincides with the speed of a vortex pair in a two-dimensional fluid.

Thus, the speed of one heton grows linearly with b at small distances b between vortices forming the heton, then it follows an algebraic decay law $\sim b^{-2}$ if the distance between vortices is larger than the local Rossby radius of deformation, but smaller than the bulk Rossby radius of deformation, and finally we have a decay law $\sim b^{-1}$ at distances larger than the bulk Rossby radius. The characteristic scale for the maximum speed of the heton is

$$C_{max}(d) = \frac{4}{3\sqrt{3}}\frac{1}{d^2}, \qquad b_{max} = \frac{d}{\sqrt{2}}, \tag{5.9}$$

for the case of $d \ll 1$. In the limit $b > \lambda_1^{-1}$, the estimation based on (5.8) gives

$$C_{max}(1) = 0.8, \qquad b_{max} = 1.11\lambda_1^{-1}. \tag{5.10}$$

The maximum propagation speed C_{max} is of the order $O(1)$ for the general case.

The structure of the flow associated with a tilted heton in the reference frame translating with the heton is given by the stream function:

$$\Psi = G(\sqrt{x^2 + (y - b/2)^2}, z, 0) - G(\sqrt{x^2 + (y + b/2)^2}, z, -d) - Cy. \tag{5.11}$$

For $b = 0$ and $d \neq 0$, we have $C = 0$, i.e. a purely baroclinic vertically aligned heton with axisymmetric streamlines. For $b \neq 0$, the tilted three-dimensional heton has a barotropic flow component, similar to two-layer (Gryanik 1983*a*; Hogg & Stommel 1985*a*) and multi-layer (Gryanik & Tevs 1989) tilted hetons. The structure of the flow is asymmetric with respect to the y-axis and is dominated by an azimuthal dipole mode. Only in the case $d = 1$ does it gain a pure dipole structure owing to the additional symmetry between upper and lower vortices (this specific property holds only for a model with constant N). A sketch of Ψ is shown in figure 3 for $b = 0.3$ and $d = 0.25$.

The fluid enclosed by the contour $\Psi(x, y, z) = 0$ migrates with the heton, see e.g. the separatrix at surface $z = 0$ in figure 3. For fixed b the anticyclonic circulation cell at the surface becomes less and less pronounced with increasing d. The characteristic horizontal and vertical scales of the volume which migrates with the heton are universal in the sense that they are independent of the strengths of vortices. This conclusion follows from the condition $\Psi = 0$ and the formula for C, see equation (5.5). The enclosed fluid which migrates with the heton gives rise to the travelling buoyancy anomaly. The buoyancy deficit $\mathscr{D}$ carried by a tilted three-dimensional heton remains the same as for a vertically aligned heton, see (5.2). Formally, this result is due to the linear superposition of the contributions from the two point vortices forming the heton. More information on the general structure of circulation

cells associated with quasi-geostrophic baroclinic three-dimensional point vortices can be found in Doronina (1995).

The distance between cyclonic and anticyclonic vortices in a tilted heton will not remain constant if it interacts with other hetons. Thus, let us consider the interaction between two hetons.

6. Interaction between two three-dimensional hetons

The motion of two three-dimensional hetons (formally, this is a four-vortex problem) has not been considered in the literature for the case of a continuously stratified fluid. We note that Hogg & Stommel (1985*a*) treated this problem in the framework of a two-layer model, with layer depths being equal, and Gryanik & Tevs (1997) considered it using a multi-layer model. For the case of two identical three-dimensional hetons the problem is amenable to complete analytical investigation (similar to the two-dimensional point vortex problem considered by Eckhardt & Aref 1988), since the system can be described by a Hamiltonian system with 8 degrees of freedom which has four common constants of motion in involution. Thus, the two three-dimensional heton problem is integrable.

6.1. *Symmetry of motion of two three-dimensional hetons*

In agreement with the general integral constraints, see (4.19)–(4.21), we have $\mathscr{P}_x = \mathscr{P}_y = 0, \mathscr{J} = 0$ and $\mathscr{I} = 0$. The first two integrals $\mathscr{P}_x = \mathscr{P}_y = 0$ give

$$(x_{c1} - x_{a1})^2 + (y_{c1} - y_{a1})^2 = (x_{c2} - x_{a2})^2 + (y_{c2} - y_{a2})^2 \equiv b^2, \tag{6.1}$$

$$(x_{c1} - x_{a2})^2 + (y_{c1} - y_{a2})^2 = (x_{c2} - x_{a1})^2 + (y_{c2} - y_{a1})^2 \equiv a^2, \tag{6.2}$$

which implies that the distances between cyclones and anticyclones remain constant during the motion. In combination with integral $\mathscr{J}$, the integrals $\mathscr{P}_x$ and $\mathscr{P}_y$ give

$$(x_{c1} - x_{c2})^2 + (y_{c1} - y_{c2})^2 = (x_{a1} - x_{a2})^2 + (y_{a1} - y_{a2})^2. \tag{6.3}$$

Finally, from equations (6.1), (6.2), (6.3) and integral $\mathscr{I} = 0$ we have

$$(x_{c1} - x_{c2})^2 + (y_{c1} - y_{c2})^2 = (x_{a1} - x_{a2})^2 + (y_{a1} - y_{a2})^2 = a^2 + b^2. \tag{6.4}$$

Thus, the motion of two hetons has a symmetry: the four vortices form a rectangle at every instant of their motion.

6.2. *Integration of equations of relative motion*

Taking into account this symmetry, let us now consider the equations of heton motion (4.13)–(4.16) for the case of two hetons. The equations of relative motion are obtained by subtracting equation (4.14) from (4.13) and equation (4.16) from (4.15). We find

$$\frac{\mathrm{d}a}{\mathrm{d}t} = -\frac{\partial}{\partial b}\left[G(\sqrt{a^2 + b^2}, 0, 0) + G(\sqrt{a^2 + b^2}, -d, -d) - 2G(b, 0, -d)\right], \tag{6.5}$$

$$\frac{\mathrm{d}b}{\mathrm{d}t} = \frac{\partial}{\partial a}\left[G(\sqrt{a^2 + b^2}, 0, 0) + G(\sqrt{a^2 + b^2}, -d, -d) - 2G(a, 0, -d)\right]. \tag{6.6}$$

A solution to the problem (6.5), (6.6) is a set of formulae giving the positions at time t in terms of the initial positions. The heton strengths and their vertical separations appear as parameters in these formulae. The problem may be reduced to quadratures, although the integrand is, in general, given only implicitly. Therefore, it

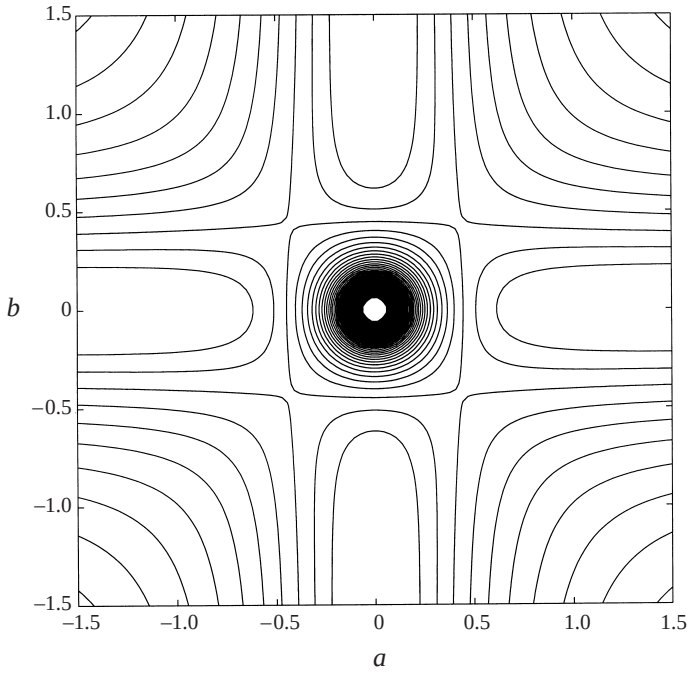

FIGURE 5. The contours of the Hamiltonian $\mathscr{H}$ for two identical three-dimensional hetons ($d = 0.5$).

is more convenient to perform an analysis of stationary states, to give a classification of feasible regimes (types of trajectories in the phase space) and then to integrate the equations numerically for representative cases.

6.3. *Classification of regimes*

Owing to the symmetry described above we find for the integral of motion

$$\mathscr{H} = -G(\sqrt{a^2+b^2},0,0) - G(\sqrt{a^2+b^2},-d,-d) + 2G(a,0,-d) + 2G(b,0,-d). \quad (6.7)$$

Except for certain special asymptotic cases which will be considered in detail later the function $\mathscr{H}$ (see the contours of $\mathscr{H}$ in figure 5) makes the algebra very complex for the general case of finite depth.

Stationary states. The stationary configurations of the vortices are obtained by setting the right-hand sides of equations (6.5) and (6.6) to zero. Owing to the symmetry, we have $a = b$ and

$$\frac{\partial}{\partial a}\left[G(\sqrt{2}b,0,0) + G(\sqrt{2}b,-d,-d) - 2G(b,0,-d)\right] = 0. \quad (6.8)$$

Finally, using an explicit expression for Green's function (4.3) we arrive at the stationary solution

$$a = b = b_*(d). \quad (6.9)$$

Thus, in the stationary state, vortices form a square with the horizontal side depending only on d.

For $d \ll 1$, that is in the limit of infinite depth, we have

$$b_* = c_* d, \qquad c_* \approx 0.86. \quad (6.10)$$

For the general case, see curve 2 in figure 6, the function $b_*(d)$ shows that with

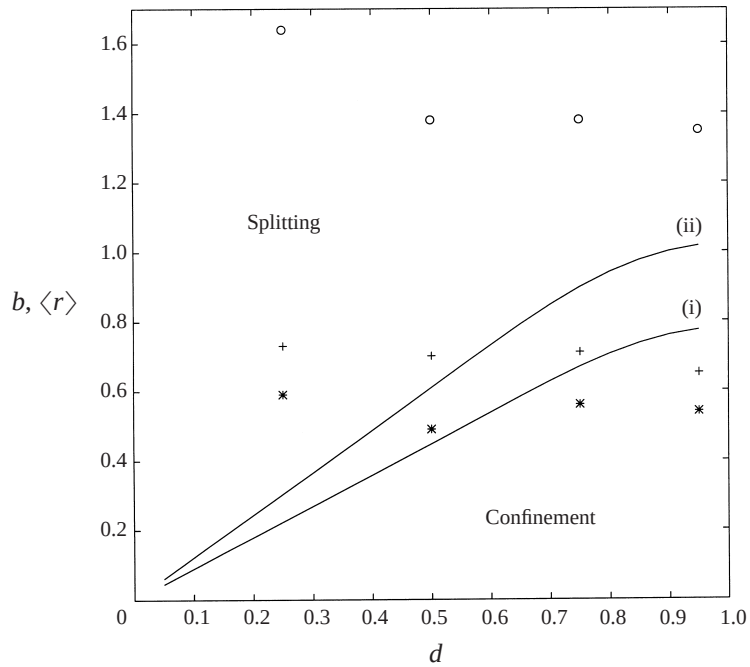

FIGURE 6. Critical separations for two three-dimensional hetons, the mean separation of three-dimensional hetons and classification of regimes. Solid lines (i) and (ii) represent b_c and $2^{1/2}b_*$, respectively. The mean separations between vortices in all experiments are denoted by ◯, runs CiDnD; +, runs CiDnR; *, runs CiDnS (the parameters of these experiments are given in table 1).

increasing d the size of the stationary square decreases with respect to the limit of infinite depth (6.10) owing to the influence of the bottom. For $d = 1$, that is when the vertical size of hetons is equal to the total depth of the fluid, we have $b_*(1) \approx 0.76$.

The stationary state is unstable, because it corresponds to the saddle point on the phase plane, as follows from figure 5. The contours of $\mathscr{H}$, depicted in figure 5, display the properties of motions in the general case when distances between vortices are arbitrary. The phase portrait is symmetric about the a- and b-axis. Nine regions are distinguished and separated by the $\mathscr{H} = \mathscr{H}_*$ contour, where $\mathscr{H}_*$ is the energy of two hetons in the stationary state

$$\mathscr{H}_* = -G(\sqrt{2}b_*, 0, 0) - G(\sqrt{2}b_*, -d, -d), +4G(b_*, 0, -d) \tag{6.11}$$

which depends only on d, that is $\mathscr{H}_* = \mathscr{H}_*(d)$. The nine regions correspond to only three different regimes of relative motion due to symmetry, which are the confinement, splitting and reconnection regimes.

Confinement regime. In the central region of the phase plane, all phase trajectories are finite since the vortex interaction is dominated by the vortices of the same level. They therefore rotate. The maximum separation between the vortices in the confinement regime is $\sqrt{2}b_*$.

Splitting regime. In the splitting regime the trajectories on the phase plane intersect the axis $a = 0$ or $b = 0$ and split at infinity, the trajectories are infinite. The behaviour of baroclinic vortices is dominated by interactions between vortices of different layers which appear to counteract the tendency of vortices with the same sign to rotate.

The minimum separation between hetons in the splitting regime is attained for

$a = 0$, $b = b_c$ or $a = a_c$, $b = 0$. Owing to symmetry, we have $a_c = b_c$, where b_c is the root of the equation

$$-G(b_c, 0, 0) - G(b_c, -d, -d) + 2G(0, 0, -d) + 2G(b_c, 0, -d) = \mathscr{H}_*. \tag{6.12}$$

For the general case, function b_c is shown in figure 6, curve (i). In the limit of infinite depth $b_c^2 + d^2 \ll 1$, it is proportional to d:

$$b_c = c_c d, \qquad c_c \approx 0.87. \tag{6.13}$$

The constant c_c is related to the constant c_* and can be calculated from (6.12) and (6.11). For $d = 1$, (6.12) gives $b_c(1) \approx 0.77$. This value for the minimum separation between hetons in the splitting regime can be compared with that for the two-layer model $b_c \approx 1.43$, which corresponds to $b_c(1) \approx 0.46$ following from (6.12) if only the barotropic and the first baroclinic modes are taken to approximate Green's function. A comparison shows that the approximation of the barotropic and the first baroclinic modes underestimates the minimum separation between hetons. The difference between the two-layer model and the barotropic and the first baroclinic modes approximation is attributed to the difference in the definition of the Rossby radii (the ratio of them is $1/\pi$).

Taking as initial state two hetons with separations $a = 0$ and $b = b_0$, the contour where $b \to \infty$ and $a \to a_\infty$ is defined by equation

$$-G(b_0, 0, 0) - G(b_0, -d, -d) + 2G(0, 0, -d) + 2G(b_0, 0, -d) = 2G(a_\infty, 0, -d). \tag{6.14}$$

For the case of infinite depth this equation shows that the maximal possible separation between vortices forming the heton a_∞ is $a_\infty = c_\infty d$. Here, c_∞ is a constant which can be calculated by setting $b_0 = b_c(d)$ and substituting it into equation (6.14). The asymptotic value

$$a_\infty = \tfrac{3}{4} d \left(\frac{d}{b_0} \right)^{5/2} \quad \text{for} \quad d \ll b_0 \ll 1, \tag{6.15}$$

shows that the finite separation between vortices in the heton decreases rapidly if the initial distance between hetons b_0 increases. The same is also true for the general case.

Reconnection regime. The remaining four regions on the phase plane correspond to reconnection regimes of vortex motion. Since the trajectories belonging to these regions intersect neither the a- nor b-axes, the hetons in these regions cannot be aligned vertically at any instant of time. Correspondingly, they are formed through exchange of vortices that initially formed other hetons.

6.4. *Absolute motion*

The phase diagram, see figure 5, gives only information on the relative motion of vortices, but not on the absolute motion. The trajectories of absolute motion of vortices remain axisymmetric during the entire evolution owing to constraints imposed by the integrals of motion.

Figure 7 shows typical examples of absolute motion in a system of two hetons placed initially at two Rossby radii (based on the fluid depth). The vertical heton scale d increases progressively from figure 7(*a*) to figure 7(*d*). The heton dynamics is strongly dependent on the local Rossby radius (based on the vertical heton scale). In figure 7(*a*), this scale is small and hetons 'feel' each other only slightly. As the height scale d grows and the local Rossby radius approaches the bulk Rossby radius, the influence of hetons on each other increases considerably (figures 7*b*–7*c*). Similarly to the case of relative motion, there are three possible regimes of motion – those of confinement,

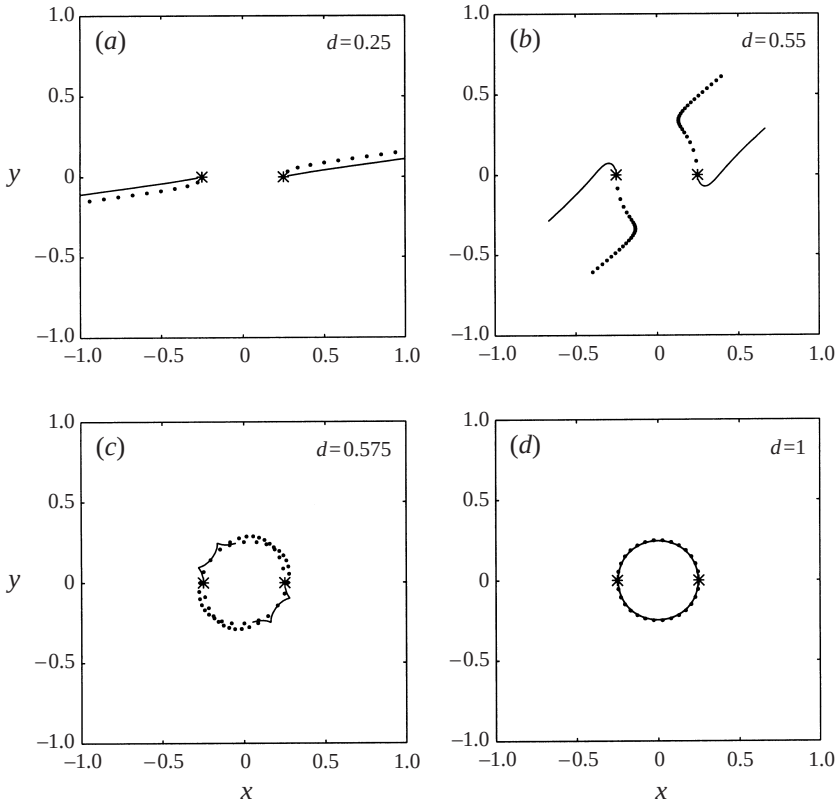

FIGURE 7. Trajectories of absolute motion of a three-dimensional heton pair for different depths. (*a*) and (*b*) represent the scattering regime, and (*c*) and (*d*) the confinement regime. Dotted lines correspond to cyclones, and solid lines to anticyclones.

splitting and reconnection. Which of them is realized depends on the initial separation between hetons. If it is less than some critical value the heton's motion will be confined provided the heton's vertical scale is sufficiently large. Otherwise, the hetons will move away from each other.

The interaction between upper vortices causes their rotation, whereas the interaction between upper and lower ones causes their self-propulsion. Upper vortices are at the surface and their interaction is effectively strengthened owing to the influence of their 'images' with respect to the boundary. This leads to prevalence of rotation at initial instants of time when the horizontal separation between the vortices composing a heton is small. Thus, initially, the heton's trajectories have a curved part. As the horizontal separation between hetons increases, the induced velocity also increases and the interaction between upper and lower layer vortices becomes more important.

Figures 8(*a*)–8(*c*) show typical examples of absolute motion at fixed $d(d = 0.5)$. Figure 8(*a*) gives an example of the reconnection regime, figure 8(*b*) of the splitting regime and figure 8(*c*) of the confinement regime.

In summary, there are three basic regimes of vortex motion, but only in the splitting and reconnection regimes do vortices form quasi-stationary three-dimensional hetons propagating with straight-line trajectories out of the region of interaction. The distance between two splitting hetons increases linearly with time ($t \to \infty$).

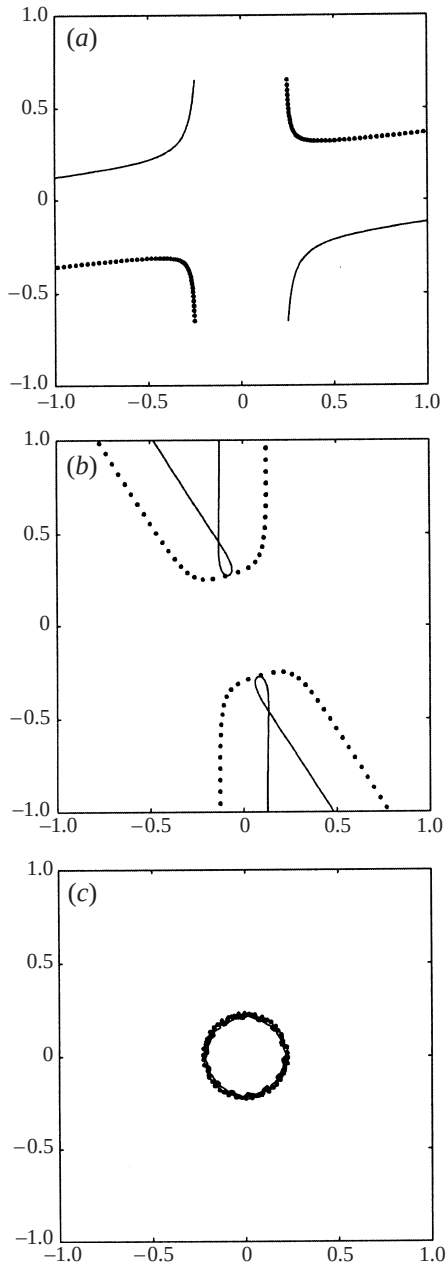

FIGURE 8. Trajectories of absolute motion of a three-dimensional heton pair for different separations. (*a*) represents the reconnection regime, ($d = 0.5$, $a = 0.5$, $b = 1.3$) (*b*) the scattering regime and ($d = 0.5$, $a = 0.25$, $b = 1.5$) (*c*) the confinement regime, ($d = 0.5$, $a = 0.15$, $b = 0.4$). Dotted lines correspond to cyclones, and solid lines to anticyclones.

7. Collisionless approximation for three-dimensional hetons

As we have mentioned in § 1, we are interested in the analysis of the spreading law of heton populations. This phenomenon is related, as we can see from the analysis in the previous section, to the dynamics of vortices in the splitting and reconnection

regimes which results in the formation of quasi-stationary three-dimensional hetons as $t \to \infty$. Let us consider this asymptotic stage of evolution in detail. We will neglect the interaction between hetons and refer to such regimes of motion as collisionless approximation, and to such populations of hetons as a dilute gas of hetons.

7.1. *Equations of motion in collisionless approximation*

To derive the equations of motion for individual hetons let us take the limit $b \ll a$ in equation (6.7). The first-order term of expansion in the small parameter $\epsilon = b/a$ gives

$$\mathscr{H} = \mathscr{H}_0(b) = G(b, 0, -d). \tag{7.1}$$

The generalization for the case of an arbitrary number of hetons is obvious. By introducing new variables $\boldsymbol{b}_i = \boldsymbol{r}_{ci} - \boldsymbol{r}_{ai}$ for the size of the heton and $\boldsymbol{r}_i = (\boldsymbol{r}_{ci} + \boldsymbol{r}_{ai})/2$ for the position of its centre we obtain the following Hamiltonian

$$\mathscr{H} = \sum_{i=1}^{\mathscr{N}} \mathscr{H}_0(b_i). \tag{7.2}$$

It is independent of individual three-dimensional heton positions and depends on d only as on a parameter. In terms of the new variables $\boldsymbol{b}_i, \boldsymbol{r}_i$ the equations of motion are

$$\frac{\mathrm{d}r_i^\alpha}{\mathrm{d}t} = \epsilon_{\alpha\beta} \frac{\partial \mathscr{H}_0}{\partial b_i^\beta}, \qquad \frac{\mathrm{d}b_i^\alpha}{\mathrm{d}t} = 0. \tag{7.3}$$

According to these equations, all hetons propagate independently with constant speeds

$$C_\alpha = \epsilon_{\alpha\beta} \frac{b_\alpha}{b} C(b, d). \tag{7.4}$$

Here, C is given by (5.4) and (5.5). Remember also that each heton carries the same buoyancy deficit $\mathscr{D}$ owing to independence of $\mathscr{D}$ on $\boldsymbol{b}_i$.

7.2. *Kinetic equation for a dilute gas of three-dimensional hetons and spreading law*

To analyse quantitatively the effects of spatial inhomogeneity in populations of large numbers of hetons, we introduce a statistical description in terms of a distribution function $f(\boldsymbol{r}, \boldsymbol{b}, \gamma, t)$. The number of hetons in the phase volume $\mathrm{d}\boldsymbol{r}\,\mathrm{d}\boldsymbol{b}\,\mathrm{d}\gamma$ at a fixed moment of time t is given by $f(\boldsymbol{r}, \boldsymbol{b}, \gamma, t)\ \mathrm{d}\boldsymbol{r}\,\mathrm{d}\boldsymbol{b}\,\mathrm{d}\gamma$. We assume that the distribution function is normalized to unity.

Using the Hamiltonian (7.1), it is easy to derive the kinetic equation for the time evolution of the distribution function following the usual procedure, see e.g. Lifshitz & Pitaevsky (1979),

$$\frac{\partial f}{\partial t} + \boldsymbol{C}(b) \frac{\partial f}{\partial \boldsymbol{r}} = 0. \tag{7.5}$$

The general solution of equation (7.5) is given by

$$f(\boldsymbol{r}, \boldsymbol{b}, \gamma, t) = f_0(\boldsymbol{r} - \boldsymbol{C}(\boldsymbol{b})t, \boldsymbol{b}, \gamma), \tag{7.6}$$

where the explicit form of $f_0(\boldsymbol{r}, \boldsymbol{b}, \gamma, t)$ is specified by the initial conditions.

For an initially localized distribution, the solution (7.6) tells us that the mean radius of the heton population for $t \to \infty$ follows the law

$$\langle R(t) \rangle = \langle C \rangle\, t, \tag{7.7}$$

where the mean radius is

$$\langle R(t)\rangle = \left(\int r^2 f_0(\boldsymbol{r} - \boldsymbol{C}(\boldsymbol{b})t, \boldsymbol{b}, \gamma)\, \mathrm{d}\boldsymbol{r}\, \mathrm{d}\boldsymbol{b}\, \mathrm{d}\gamma \right)^{1/2}, \tag{7.8}$$

and the mean speed is

$$\langle C\rangle = \left(\int \boldsymbol{C}^2(\boldsymbol{b}) f_0(\boldsymbol{r}, \boldsymbol{b}, \gamma)\, \mathrm{d}\boldsymbol{r}\, \mathrm{d}\boldsymbol{b}\, \mathrm{d}\gamma \right)^{1/2}. \tag{7.9}$$

Equation (7.7) will be referred to further as the spreading law for the heton population. Applied to the problem of heat and passive scalar transport, this law implies the upper 'advective' bound for superdiffusion, see e.g. Isichenko (1992). It differs from the ordinary diffusion law $\langle R\rangle \propto \sqrt{t}$.

It is straightforward to show that the variance of the mean radius of a heton population follows the linear growth law too. Indeed, hetons of different sizes move with different velocities, these velocities approach respective constant values as the separation between hetons increases and then the distance between them will be a linear function of time. It is also clear that the mean radii and variances of all geophysical fields connected with the heton population will follow the same spreading law at large time.

Clearly, the kinetic equation can only be applied to analyse the spreading of a heton population for times greater than the characteristic time of the development of all types of instabilities leading to the formation of individual non-interacting hetons.

7.3. *Estimation of* $\langle C\rangle$

Let us estimate the mean propagation speed. If hetons are uniformly distributed on a circumference of radius R and all have equal intensities γ_0 and sizes $b = b_*$ that correspond to the maximal heton size in the splitting regime the distribution function is

$$f_0 = \frac{1}{4\pi^2 R b_*}\delta(r - R)\delta(\gamma - \gamma_0)\delta(b - b_*). \tag{7.10}$$

Obviously, in this case, equation (7.9) gives $\langle C\rangle = C(b_*(d), d) = C_*(d)$. In the limit of infinite depth ($d \ll 1$) we have, see (6.10) and (5.6),

$$\langle C\rangle = C_*(d) \approx 0.75\frac{1}{d^2}, \tag{7.11}$$

where the coefficient of proportionality follows from (6.10). If we take $b = b_{max}$ which corresponds to the maximal propagation speed, the coefficient of proportionality in (7.11) is given by (5.9) and is equal to $4/3\sqrt{3} \approx 0.77$.

Hetons in the splitting regime can have different sizes from 0 to b_*, see §6 and figure 3. In this case, the mean speed $\langle C\rangle$ will depend on the distribution of sizes. If we take this distribution to be uniform between 0 and $b_*(d)$

$$f_0 = \frac{1}{2\pi^2 R b_*^2}\delta(r - R)\delta(\gamma - \gamma_0)[\Theta(b) - \Theta(b_* - b)], \tag{7.12}$$

(7.9) gives

$$\langle C\rangle = \alpha(d) C_*(d), \tag{7.13}$$

where

$$\alpha(d) = \left[2\int_0^1 \left(\frac{C(x,d)}{C_*(d)} \right)^2 x\, \mathrm{d}x \right]^{1/2}, \tag{7.14}$$

see Appendix D for details. The propagation velocity $C_*(d)$ is the only relevant velocity scale for a heton, which contains the information about mutual interaction between two hetons. Therefore, it appears in the scaling, and the coefficient of proportionality $\alpha(d)$ accounts for the distribution of hetons over sizes and directions of propagation.

In the case of infinite depth using (7.14) and (7.11) we obtain

$$\langle C \rangle \approx 0.69 C_*(d) \approx 0.52 \frac{1}{d^2}, \tag{7.15}$$

since

$$\alpha \approx 0.69 \tag{7.16}$$

is a constant (see Appendix D) in this approximation. In the general case, function $\alpha(d)$ deviates only slightly from the asymptotic value given by (7.16) in the range $0.8 < d < 1$.

It is also clear that the deviation of the distribution function over sizes b from a uniform one which increases the number of hetons with small sizes results in reducing the magnitude of $\alpha(d)$ and vice versa the increase in the number of hetons with sizes b of the order b_* results in an increase of $\alpha(d)$, see Appendix D. The extreme limit $b = b_*$ for all hetons results in (7.11). Moreover, $\alpha(d)$ decreases also if only a fraction of hetons P take part in the splitting and the remaining $1 - P$ hetons pass into the confinement regime of motion. A simple distribution function describing such a heton population can be defined by

$$f = P f_0 + (1 - P) \frac{1}{4\pi^2 R b} \delta(r - R) \delta(\gamma - \gamma_0) \delta(b), \tag{7.17}$$

where the function f_0 is given by (7.12) and the last term represents the hetons in the confinement state. This latter term does not contribute to the integral (7.9), because $C(0) = 0$. So, the mean propagation speed is given by (7.13) multiplied to P. It is difficult to estimate P analytically, because of a persistence of both a highly correlated heton-like dynamics and a chaotic dynamics of a sea of individual vortices in confinement regimes. The baroclinic instability theory has been used for the treatment of a special averaged heton population. It obviously gives $P = 1$ for unstable states and $P = 0$ for stable states. In general, we can expect $P \to 1$ for well-pronounced splitting regimes and $\frac{1}{2} < P < 1$ when splitting regimes of heton motions control the spreading of the population. We will confirm this suggestion calculating P numerically in the next section.

Formally speaking, (7.7) and (7.13) can be interpreted as a spreading law of independent 'equivalent' hetons with 'equivalent' strength $\gamma_* = \alpha P \gamma$, propagating in a radial direction with speed $C_*(d)$. Numerically, $C_*(d)$ is very close to the maximum propagation velocity of a single heton $C_{max}(d)$ derived above.

In the next section, we will investigate the linear spreading law and estimate the spreading rate of heton populations in the general case where the interactions between hetons are taken into account by numerical experiments.

8. Numerical experiments with a three-dimensional heton model

In this section, we will consider the behaviour of an ensemble of three-dimensional hetons in two kinds of models. First, initial-value problems describing the evolution of heton populations are considered. Secondly, models with random heton sources are addressed, in which new hetons are created within the generation area at a fixed rate.

Experiment	$d = h/H$	R_{hor}/L_h	Symbol	Realizations
CiD1D	0.25	15	○	10
CiD2D	0.5	7.5	○	10
CiD3D	0.75	5	○	10
CiD4D	1.0	3.75	○	10
CiD5D	0.2	18.75	○	10
CiD6D	0.28	13.39	○	10
CiD7D	0.33	11.36	○	10
CiD1R	0.25	15	+	10
CiD2R	0.5	7.5	+	6
CiD3R	0.75	5	+	6
CiD4R	1.0	3.75	+	4
CiD5R	0.2	18.75	+	10
CiD6R	0.28	13.39	+	10
CiD7R	0.33	11.36	+	10
CiD1S	0.25	5	*	4
CiD2S	0.5	2.5	*	4
CiD3S	0.75	1.67	*	4
CiD4S	1.0	1.25	*	4

TABLE 1. Nomenclature of the experiments: Ci denotes the circumference geometry of a cooling region, D1–D7 refer to different mixing depths, and the last letter indicates runs with pulse forcing (D) or long-time forcing (R, S). The last column is the number of experiments used for averaging. For all runs, $N/f = 2$ and forcing proceeds at a constant rate, so that 121 hetons are created during 1.03 units of non-dimensional time.

In our numerical simulations, hetons are placed randomly on a ring-like boundary of the cooling region. Parameters for all experiments are defined in table 1.

In the beginning of this section we also describe numerical simulations of the dynamics of five three-dimensional hetons to develop some intuition about the basic regimes that may occur simultaneously during the evolution of heton populations and about the quantification of these regimes.

8.1. *Example of multi-heton dynamics*

First, we consider the results of numerical simulations of three-dimensional heton population dynamics with five hetons, see figure 9. Figures 9(*a*) and 9(*b*) show in their lower left-hand corner two circles which illustrate the size of the bulk Rossby radius ($L = 1$) and local Rossby radius ($L_h = d \leqslant 1$). In case *a* we have $d = 0.25$, in case *b* we have $d = 1$.

Case *a* corresponds to the situation when initially three of the vertically aligned hetons (3, 4, and 5) are located within the bulk Rossby radius but have separations bigger than the local Rossby radius. Because of mutual interaction the hetons become tilted and start to propagate in straight lines out of the regions of their initial locations. During the propagation, heton 3 becomes close to hetons 1 and 2, which initially were separated by a distance greater than the bulk Rossby radius. Heton 3 then induces their tilting and motion. Owing to this interaction, the trajectories of hetons 1 and 2 are nearly perpendicular to the trajectory of heton 3. The trajectories of the fast moving hetons 4 and 5 are straight all the time. The described dynamics is typical for the splitting regime of motion.

In case *b* the initial positions of the hetons are the same as above, but the mixing depth is four times larger. In this case, the dynamics alters drastically: the group of

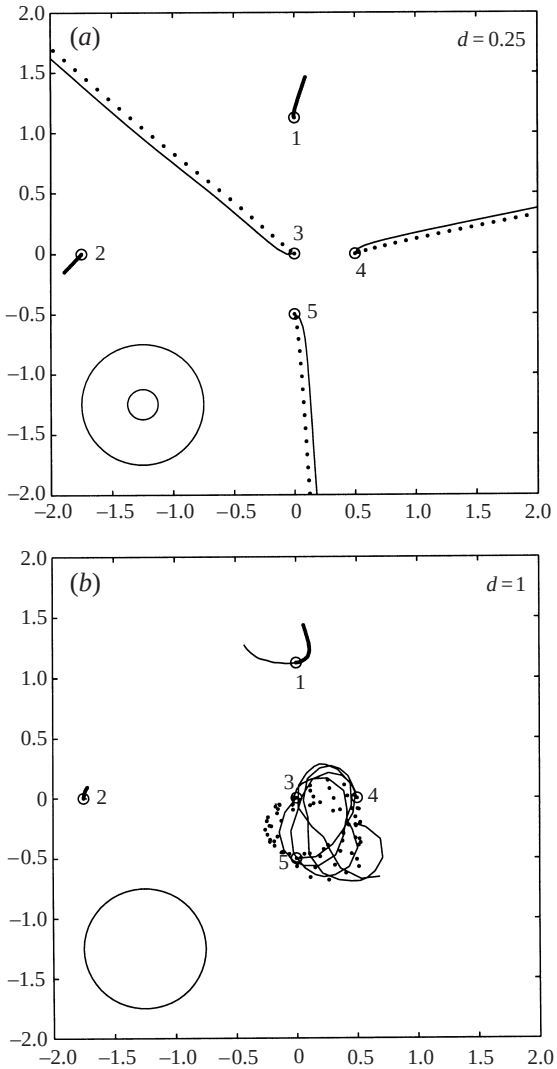

FIGURE 9. Trajectories of absolute motion (dotted lines correspond to cyclones, and solid to anticyclones) for five three-dimensional hetons. Initial positions are: $x_1 = 0$, $y_1 = 1.25$; $x_2 = -1.75$, $y_2 = 0$; $x_3 = 0$, $y_3 = 0$; $x_4 = 0.5$, $y_4 = 0$; $x_5 = 0$, $y_5 = -0.5$.

three hetons (3, 4, and 5) that were in a splitting regime of motion now fall into the confinement regime, because now the separation between them is smaller than the local Rossby radius. All vortices forming the hetons rotate in a region of finite size. One of the two remaining hetons (1), the closest to the rotating group, becomes influenced and propagates away from the rotating group (note that the trajectory of heton 1 is very different if compared to the preceding case). Heton 2 remains practically insensitive to the changes in dynamics of the other vortices because its separation remains bigger than the bulk Rossby radius.

Summarizing, the dynamics of heton populations depends on the relation between three typical scales associated with the problem – the bulk Rossby radius ($L = 1$), the local Rossby radius ($L_h = d \leqslant 1$) and the typical separation between the hetons (L_{hor}). If the minimum distance between hetons (inside the population) exceeds the

bulk Rossby radius, their behaviour is predominantly splitting. If it is less than the local Rossby radius, hetons are in a confined regime of motion. All regimes can coexist simultaneously.

8.2. *Quantification*

The evolution of a heton population will be described by the following function

$$P_{c,a}(t) = 1 - \left(\int Q_{c,a}(x, y, z, t)\, \mathrm{d}x\, \mathrm{d}y\, \mathrm{d}z \right)^{-1} \left(\int_{\mathscr{G}} Q_{c,a}(x, y, z, t)\, \mathrm{d}x\, \mathrm{d}y\, \mathrm{d}z \right), \tag{8.1}$$

where indices c, a refer to cyclonic and anticyclonic vortices, respectively, the region $\mathscr{G}$ corresponds to the generation area of the vortices. So, the functions $P_{c,a}(t)$ describe the fraction of hetons outside the generation area, and will be used to classify the regimes of motion of heton populations. If the hetons are in the splitting regime, $P_c(t) \approx P_a(t)$ will tend to unity. In the opposite limit, the confinement regime, $P_{c,a}(t) \to 0$.

Another characteristic function is the mean radius of the heton population

$$\langle R_{c,a}(t) \rangle = \mathscr{N}^{-1} \sum_{c,a} \sqrt{x_{c,a}^2 + y_{c,a}^2}. \tag{8.2}$$

The time dependence of the mean radius defines the law of horizontal PV transport due to heton motion. The variance $\sigma_{c,a}$ of the mean radius defined as

$$\sigma_{c,a}(t) = \left(\frac{1}{\mathscr{N} - 1} \sum_{c,a} (x_{c,a}^2 + y_{c,a}^2 - \langle R_{c,a} \rangle^2) \right)^{1/2}, \tag{8.3}$$

characterizes the width of the frontal zone.

One more characteristic of interest is the mean separation $\langle r \rangle$ between hetons in the generation region defined as

$$\langle r \rangle \equiv \left(\frac{2\pi R_{hor}}{\mathscr{N}_g} \right)^{1/2}, \tag{8.4}$$

where $R_{hor} = L_{hor}/L$ is the characteristic non-dimensional horizontal scale, see (4.11), $L = NH/f$ is the bulk Rossby radius, see (4.8), and $\mathscr{N}_g$ is the number of hetons inside the area $2\pi L_{hor} L$. This parameter is the measure of intermittency of the PV field in the region of generation of hetons.

8.3. *Pulse forcing*

Figures 10–13 illustrate the behaviour of hetons as observed in runs CiD1D to CiD4D. In all these runs, 48 hetons are distributed randomly on the circumference of the radius $R_{hor} = R_0$, at an initial time $t = 0$, to simulate a pulse forcing. Parameters of these runs are given in table 1.

The effect of the mutual interaction between hetons is inhomogeneous throughout the array owing to the random character of the distribution at initial time. This leads to the inhomogeneous character of their motion and splitting.

The four runs were performed for different vertical separations (mixing depths) between vortices in a heton. Since this parameter controls the local Rossby radius, the behaviour of hetons is considerably different in these four runs. In experiment CiD1D (see table 1 and figure 10), the mixing depth $d = 0.25$ is the smallest of all runs in the series. In this case the local Rossby radius is relatively small compared with the typical horizontal separation between hetons ($\langle r \rangle = 1.6$, figure 6). Therefore,

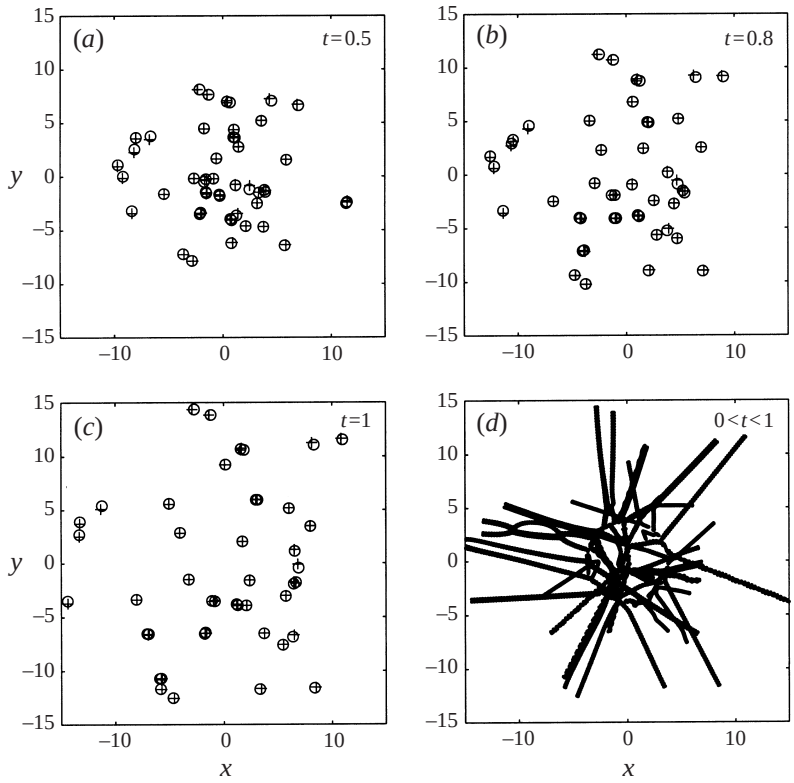

FIGURE 10. Experiment CiD1D. (*a*)–(*c*) represent distributions of hetons at different instants of time, and (*d*) trajectories for the indicated interval of integration (◯, cyclones; +, anticyclones).

the hetons are mostly in the splitting regime and leave the circumference as time progresses. Notice that hetons leave the region of generation as single entities, not as clusters.

In experiments CiD2D and CiD3D, see figures 11 and 12, the local Rossby radius is increased and we observe a tendency to clustering: hetons tend to combine in groups and then leave the region of generation. There are clusters with different numbers of hetons. Typically, they are composed of four vortices in run CiD2D (see figure 12*b*) and of four to six vortices in run CiD3D (see figure 12*c*). The interaction mechanism at large time appears to be dominated by the individual heton clusters. The speed of these heton clusters is smaller than the speed of the original hetons, because of the larger separation between the centres of the PV distributions in each cluster.

For run CiD4D the mixing depth d is the largest of all runs in the series, and the local Rossby radius equals the bulk Rossby radius. In this case $\langle r\rangle \approx 1$, and all hetons are temporarily in the splitting/confinement regime of motion, see figure 13.

For all our experiments, we have

$$P_c(t) \approx P_a(t) \approx \frac{\mathcal{N}_{out}(t)}{\mathcal{N}} \equiv P(t), \tag{8.5}$$

where $\mathcal{N}_{out}$ is the number of hetons outside the area of generation $\mathcal{G}$. Equality of $P_c(t)$ and $P_a(t)$ means that spreading is due to hetons. We analysed the behaviour of $P(t)$ as a function of time for all four runs. In the first experiment, $P(t)$ grows monotonically and approaches unity, which means that all hetons leave the region

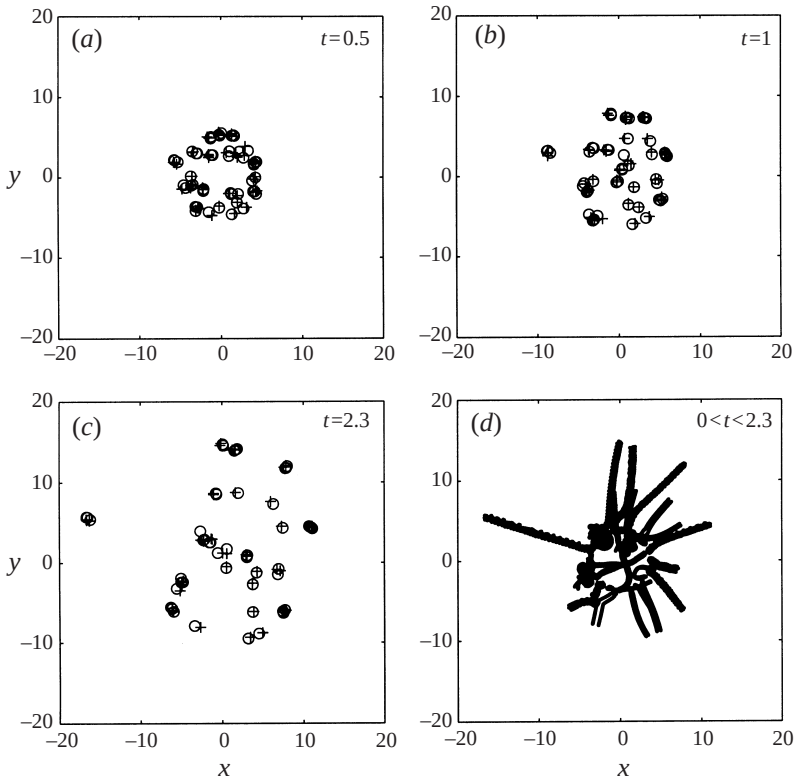

FIGURE 11. As in figure 10 but for experiment CiD2D.

of generation at large time. In the three other runs CiD2D to CiD4D, the growth is slower. For the time considered, $P(t)$ reaches only a value close to 0.7, since, as shown in figures 11 and 10, there are hetons that move inside the circumference of heton generation. The lowest level of $P(t)$ was observed in run CiD4D, which is a consequence of the fact that hetons in this run are in a confinement regime.

In experiment CiD1D, the distance between hetons increases as they move away from the generation region, and thus one may expect that the dynamics of the hetons moving into exterior regions will resemble the individual heton behaviour in an infinite domain. Experiments show that the mean radii for cyclonic and anticyclonic distributions of vortices almost coincide. Figure 14 shows a linear growth in time of the mean radius of the domain. A linear law of growth is also observed in experiments CiD2D and CiD3D, however, the rate of growth is noticeably smaller. In experiment CiD4D, hetons are in the confinement regime. Figure 14 shows that there is a slow growth of the mean radius even in that case.

Linear growth with time is also seen in the time dependence of the variance in runs CiD1D to CiD3D, where the heton populations are in a spreading regime, see figure 14. In the case of confinement, CiD4D, the variance also grows, but according to a slower law.

8.4. *Long-time forcing at a constant rate*

Now, we assume a model-forcing similar to that of Legg & Marshall (1993), but our constraint on newly created hetons is based on the local Rossby radius. Thus, the intensity of the hetons is constant, and the initial coordinates are random, with the

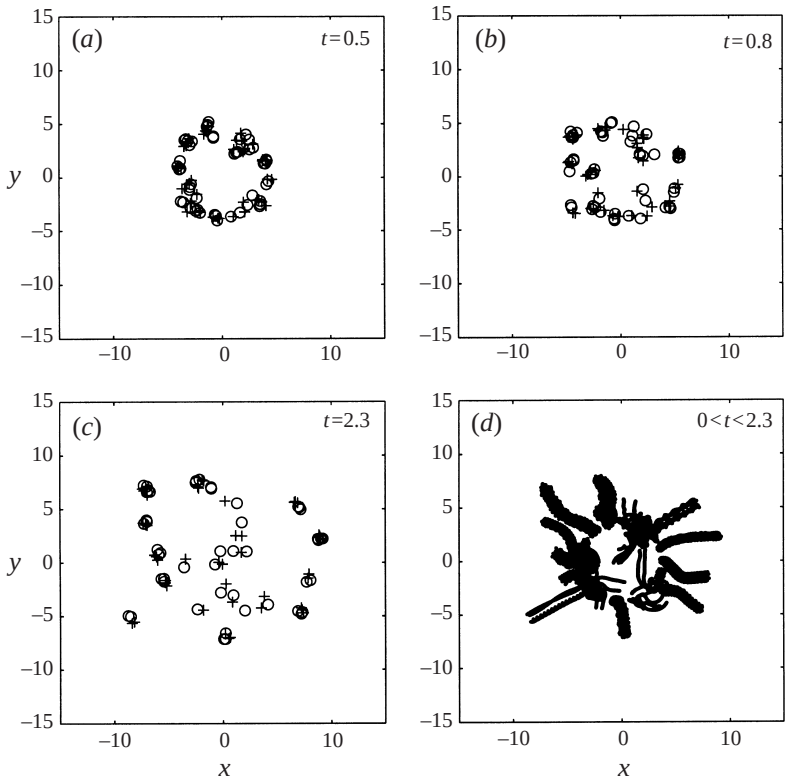

FIGURE 12. As in figure 10 but for experiment CiD3D.

additional constraint that newly created hetons must be at a larger distance from the already existing hetons than the local Rossby radius. For the sake of simplicity, we also assume a constant forcing rate, so that $t_i = i\Delta\tau$ for $0 < t_i < t_{force}$, where $\Delta\tau$ is the characteristic time interval between the generation of two hetons, and t_{force} is the forcing time. The runs CiD1R to CiD4R were performed for the same ring-like geometry as the previous runs, but this time with the forcing specified above. Parameters of these runs are given in table 1.

The behaviour of hetons is illustrated in figures 15 to 18. If compared to the corresponding experiments of the model with pulse forcing, the figures show that the circumference region is much more pronounced, since hetons are supplied to this region during the experiments. Experiment CiD1R (figure 15) is characterized by heton spreading, however, the rate of spreading is slower than in the case of pulse forcing. In the other experiments (CiD2R to CiD4R), we may observe cluster formation, but, in contrast to the experiments with pulse forcing, the main group of hetons is ultimately in a confinement regime. Only in experiment CiD1R does $P(t)$ reach a value of 0.7, whereas in the other cases it stays close to 0.5 until aggregation begins, and then increases slightly to 0.56.

The same qualitative behaviour can be inferred from plots of the time dependence of the mean radius, see figure 19. Comparing these plots with those of the radius variance (also in figure 19) we can see that for the runs CiD2R to CiD4R (which are in a confinement regime also at large time) the variance is greater than the mean radius itself.

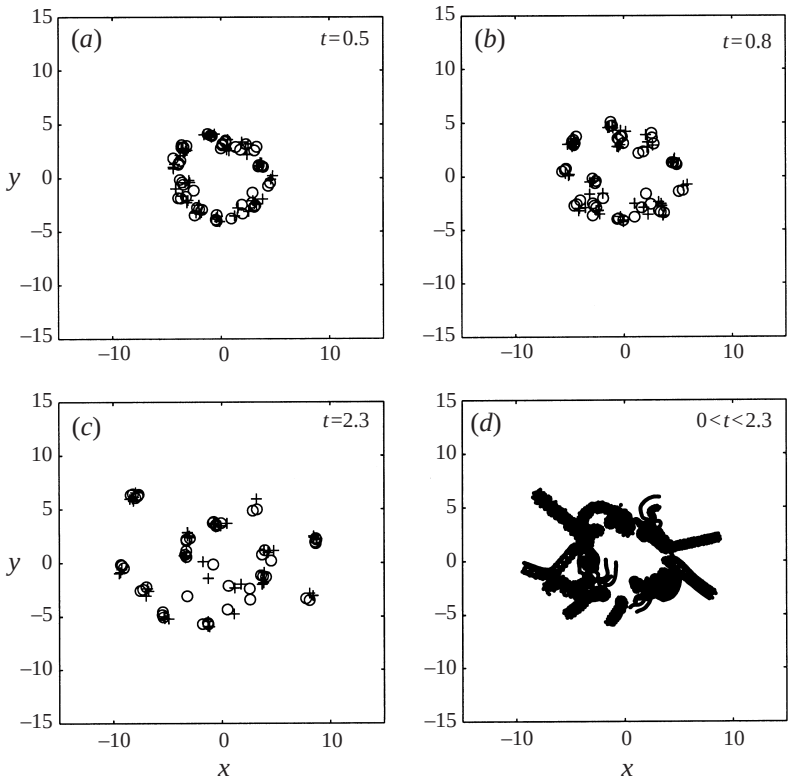

FIGURE 13. As in figure 10 but for experiment CiD4D.

We have performed series of additional runs (from 4 to 10 depending on the parameters of the experiments, see table 1) with different random realizations of initial positions of hetons (pulse forcing experiments) or of the random positions of newly created hetons (long-time forcing experiments). The additional series of experiments were performed also to cover a larger region in parameter d, see experiments CiD5D to CiD7D and CiD5R to CiD7R in table 1 (pictures not shown). Moreover, we have performed experiments with a circumference of smaller radius (see experiments CiD1S to CiD4S in table 1, pictures not shown) to examine the effect of the parameter R_{hor}/L_h. All of the experiments show a behaviour similar to that described above.

The analysis of numerical experiments is given in §§ 9 and 10.

9. Basic regimes

The instantaneous dynamics of a heton population cannot be interpreted in terms of a single regime of the heton pair dynamics. All fundamental regimes of mutual interaction between two hetons, splitting, confinement and reconnection (see §§ 6 and 7), take place simultaneously. Their relative importance depends on two parameters: the mean separation between hetons non-dimensionalized with the bulk Rossby radius $\langle r(t)\rangle$ and the ratio d of local to bulk radii. As time progresses, the population of hetons in a confinement regime (in the sense that there were no hetons or heton clusters self-propagating out of the region of generation) can form clusters and pass

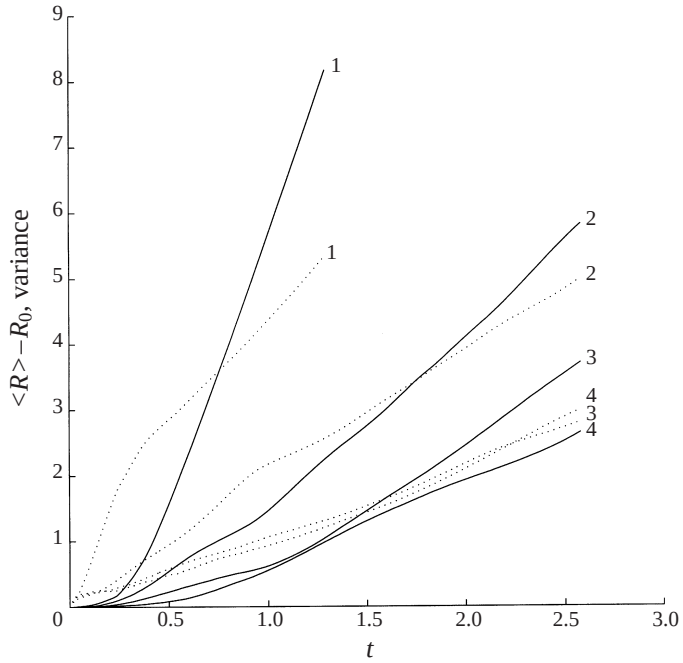

FIGURE 14. The functions ——, $\langle R \rangle$ and ·····, σ (dotted line) represent the mean radius and variance of the mean radius of the different heton populations, respectively. Experiments: 1, CiD1D; 2, CiD2D; 3, CiD3D; 4, CiD4D.

on to a splitting regime (hetons or heton clusters self-propagate out of the region of generation).

It turns out that curves $b_c(d)$ and $\sqrt{2}b_*(d)$, see figure 5, computed for the two-heton regimes can also be employed to make suggestions about the dynamical regimes of a whole heton population. This can be done by comparing the mean separation $\langle r(t) \rangle$ with these two curves. In all cases studied by us, values of $\langle r(t) \rangle$ above $\sqrt{2}b_*(d)$ corresponded to splitting regimes, and values below $b_c(d)$ to confinement regimes. As an illustration, we show the regimes at $t = 1.03$ in figure 6. The series of experiments presented by circles corresponds to the heton distributions of the runs CiD1D to CiD4D. The runs CiD1D to CiD3D are above the critical curve, and the hetons in these experiments are in a splitting regime, as can be seen from figures 10–12. The last experiment of this series CiD4D is precisely on curve 2 and can be attributed to the intermediate case of the splitting/confinement regime, as can be seen from figure 13. In experiments with forcing at a constant rate (runs CiD1R to CiD4R marked by + in figure 6), the mean distance between hetons is smaller (for a given generation rate) if compared to runs with pulse forcing. With an increase of the parameter d, the hetons enter the confinement regime. The series plotted by stars refers to experiments CiD1S to CiD4S with a circumference of smaller radius. Since the heton generation rate remains the same, the mean separation between the vortices decreases, and the confinement regime becomes more pronounced.

Both regimes – the splitting and confinement regime – were documented in laboratory experiments with circle geometry of the cooling region (Helfrich & Battisti 1991; Narimousa 1998; Boubnov & Rhines (1999, personal communication)).

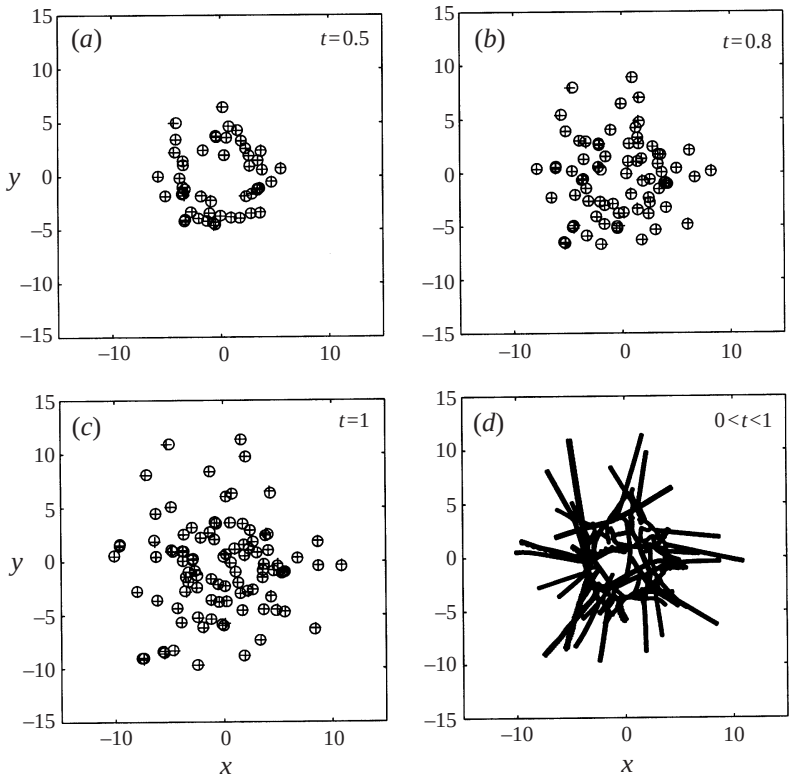

FIGURE 15. As in figure 10 but for experiment CiD1R.

10. Spreading law for a heton population

In our numerical experiments with ring-like populations, we have observed that hetons spread out from the region of generation according to

$$\langle R\rangle - R_0 \propto t, \tag{10.1}$$

for $t \to \infty$, see figures 14 and 19. As demonstrated in figure 20 the spreading rate depends sharply on the depth d, for $d < 0.8$ we have approximately $\langle C\rangle \propto d^{-2}$.

Under the assumption of a weak interaction between individual hetons this linear growth law for the mean radius of a heton population and the dependence of the spreading rate $\langle C\rangle$ on d follow from the kinetic equation in collisionless approximation, see § 8.

Based on the results of § 8, it is also natural to assume that the spreading rate scales with the characteristic speed of an individual heton. For the latter, we choose the speed $C(b_*(d), d)$ of the heton whose vortices are separated by the maximum distance $b = b_*(d)$ possible in the splitting regime, which is given by equation (5.5). In figure 20 this hypothesis is tested against numerical data. It is seen that the characteristic speed of a single heton $C(b_*(d), d)$ given by curve 1 overestimates the real spreading speed. However, all points are grouped around the regular curve 2 (which corresponds to the experiments with pulse forcing) and the regular curve 3 (experiments with long-time forcing at a constant rate) independent of the fact that they refer to different regimes and initial data. This behaviour implies that the characteristic speed of a single heton

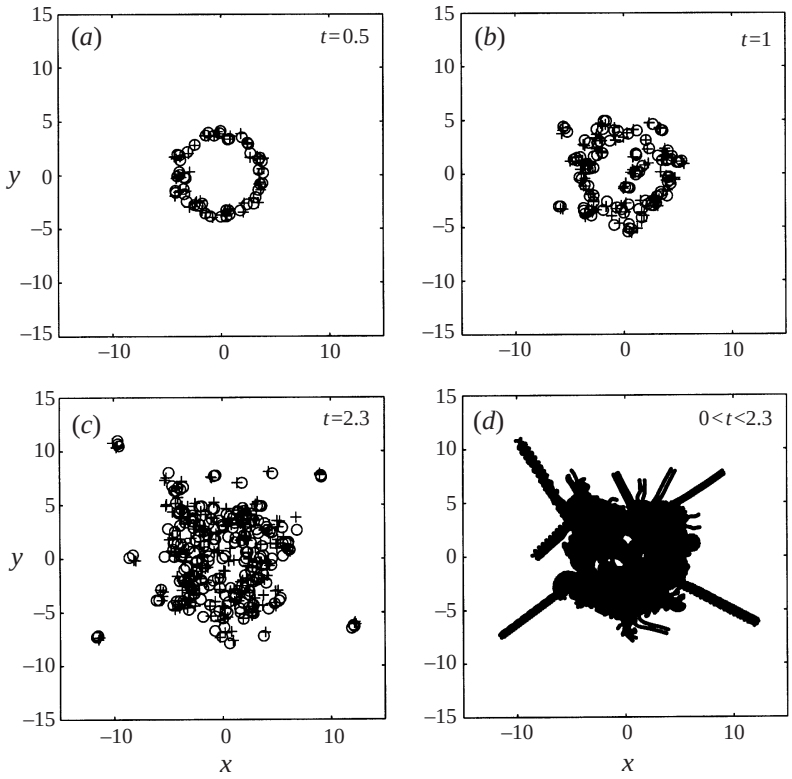

FIGURE 16. As in figure 10 but for experiment CiD2R.

gives a fairly close physical estimation for the speed in the spreading law:

$$\langle R(t)\rangle = \alpha C(b_*(d), d)t, \tag{10.2}$$

where α is a numerical constant.

We found $\alpha = 0.75$ for runs with pulse forcing (curve 2) and $\alpha = 0.25$ for runs with long-time forcing at constant rate (curve 3). The first value is very close to that found in the collisionless approximation under the assumption of a uniform distribution of heton sizes b between 0 and the maximum size for the splitting regime b_*, see equation (D 2). The applicability of the collisionless approximation for the explanation of these experiment is quite natural. According to figures 10–13 and figure 5, the hetons in these cases are indeed in the splitting regime, and the separations between hetons are large enough for the interaction between them to be weak. The difference between the theoretical and numerically found values of α can be attributed to the deviation of the distribution function of hetons over sizes from a uniform one in numerical experiments.

The other case of long-time forcing at a constant rate (represented by curve 3) requires a more careful interpretation. In these experiments, the number of hetons is small at the initial stage and the interaction between them is therefore weak. These hetons are in a splitting regime, similar to that shown in figure 7(*a*), and form the spreading part of the heton population. At this stage, the mean separation between hetons is larger than in the experiments with pulse forcing, the interaction between the hetons is weaker, and the resultant displacements of the vortices forming a heton

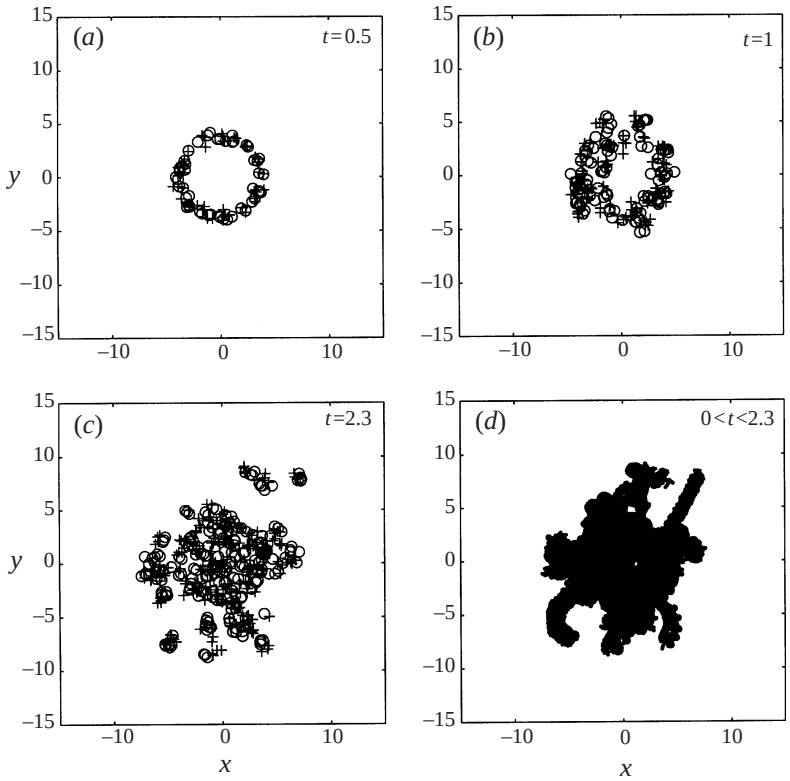

FIGURE 17. As in figure 10 but for experiment CiD3R.

is smaller, and so is their propagation speed. As the number of hetons increases with time, the number of hetons with small sizes also increases, since at the instant of generation all new hetons are aligned vertically, this results in a temporal shift of the maximum of the distribution function toward smaller scales. Hetons with smaller b propagate more slowly. As a result, we have a decrease of the magnitude of $\alpha(d)$, and finally a decrease of the rate of spreading in runs with long-time forcing at constant rate in comparison to runs with pulse forcing. Moreover, some of the hetons can pass into the confinement regime and do not leave the region of generation, compare figures 8(b) and 16. This results in an additional decrease of the magnitude of $\alpha(d)$, and the rate of spreading.

11. External scaling and spreading of chimneys in the ocean

Let us now consider the application of the three-dimensional heton theory to the problem of lateral spreading of chimneys in the ocean and in corresponding laboratory experiments. This requires the quantification of the spreading law in terms of external parameters usually used in deep convection numerical modelling and in laboratory experiments. Such a quantification depends on the problem under consideration.

Here, we consider the problem of chimney equilibration, see e.g. Legg *et al.* (1996) and Visbeck *et al.* (1997). Equilibration occurs because of the balance between the buoyancy flux through the upper surface of a localized cooling region and the lateral buoyancy transport by baroclinic vortices. We assume a ring-like geometry of the

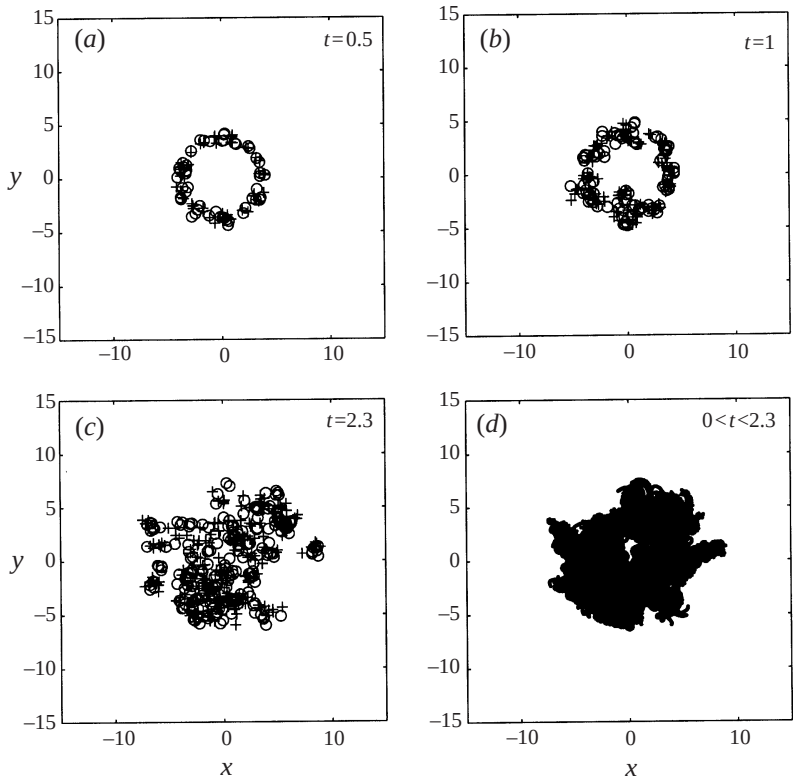

FIGURE 18. As in figure 10 but for experiment CiD4R.

cooling region, as in our numerical experiments. Moreover, we suppose that the lateral buoyancy transport is produced only by three-dimensional hetons.

In our quasi-geostrophic theory the basic parameters are: the heton strength γ, the mixing depth h and the forcing rate specified by the time interval Δt. The vortex strength γ is related to the heat/buoyancy release by equation (2.17). When the mixing agents are populations of geostrophically adjusted plumes, the buoyancy release $\overline{\mathscr{B}}$ can be estimated to be B_0/h, where B_0 is the surface buoyancy flux. The size of the geostrophically adjusted plume can be estimated to be some fraction of the Rossby radius $(N/f)h$, and the mixing time τ (the time to mix the stratified fluid of depth h) to be $N^2h^2/2B_0$. Estimating Δt to be $\mathscr{D}/B_0A$, where $\mathscr{D}$ is the buoyancy deficit per heton defined by (5.2) and A is the area of the heat input, and finally using all these estimations we obtain

$$\gamma = \alpha_\gamma \frac{N^2}{f} h^3, \tag{11.1}$$

and

$$\mathscr{N} = \left[\frac{t}{\Delta t}\right], \qquad \Delta t = \alpha_\Delta \frac{N^4 h^4}{\pi f^2 B_0 (R_{out}^2 - R_{in}^2)}, \tag{11.2}$$

where the square brackets denote the integer part, R_{in} and R_{out} are the inner and the outer radii of the ring considered in our numerical experiments, $A = \pi(R_{out}^2 - R_{in}^2)$ is the corresponding area of the heat input, and α_γ and α_Δ are constants.

Taking these estimations, we are now able to calculate all geophysical fields and the

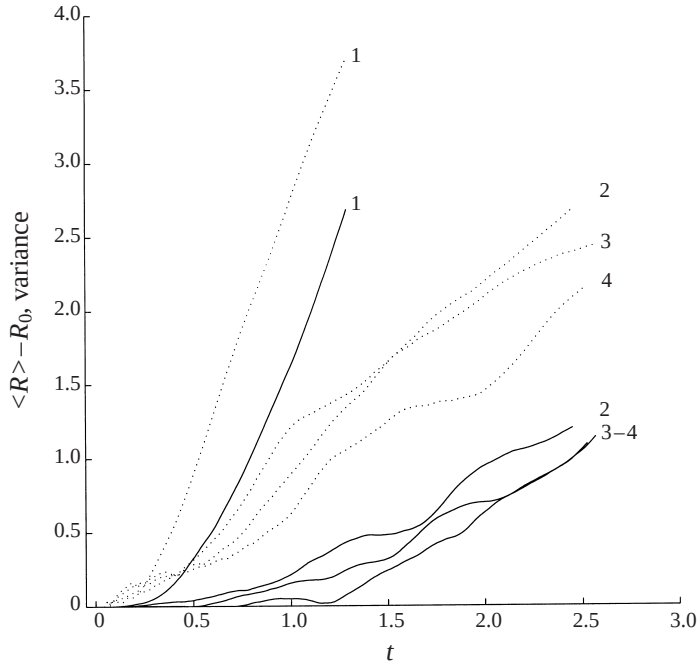

FIGURE 19. The functions ——, $\langle R \rangle$ and ·····, σ represent the mean radius and variance of the mean radius of the different heton populations, respectively. Experiments: 1, CiD1R; 2, CiD2R; 3, CiD3R; 4, CiD4R.

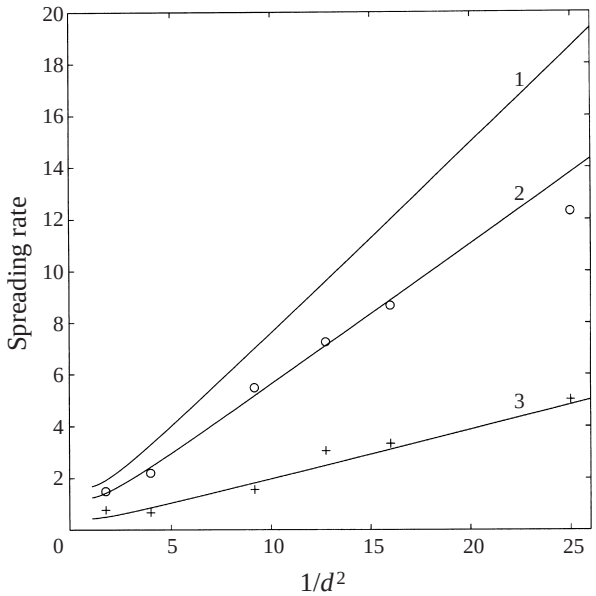

FIGURE 20. Dependence of the spreading rate $d\langle R \rangle/dt$ on $1/d^2$ normalized with $\gamma f/4\pi NH^2$. Curve 1 represents the normalized speed of a single heton, whereas curves 2 and 3 correspond to the same curve multiplied by a factor 0.75 and 0.25 and are fits for the experimental points of ○, runs CiD1D to CiD4D and runs +, CiD1R to CiD4R, respectively.

speed of propagation of three-dimensional hetons in terms of the external parameters N, f, R_{out}, R_{in}, B_0 and h.

The parameter h can be determined from the stationary buoyancy balance equation of the cooling region

$$\int B_0 \, \mathrm{d}A = \iint [\boldsymbol{J} \, \mathrm{d}\boldsymbol{l}] \, \mathrm{d}z, \tag{11.3}$$

where $\boldsymbol{J}$ is the buoyancy flux through the lateral boundary.

Since the flux due to three-dimensional hetons can be estimated by

$$\boldsymbol{J} = \boldsymbol{C}\overline{\eta}, \tag{11.4}$$

where $\boldsymbol{C}$ is the characteristic propagation speed of hetons and $\overline{\eta}$ is the mean buoyancy, the equilibrium balance equation (11.3) can be written as

$$B_0\pi \left(R_{out}^2 - R_{in}^2\right) = 2\pi \left(R_{out} C_{out} \overline{\eta}_{out} + R_{in} C_{in} \overline{\eta}_{in}\right) h, \tag{11.5}$$

where C_{in} and C_{out} are the characteristic velocities on the corresponding boundaries, and $\overline{\eta}_{in}$ and $\overline{\eta}_{out}$ are the corresponding mean buoyancies. If we assume the characteristic propagation speed $C_{out} \sim C_{in}$ to be equal to the mean speed of the hetons

$$\langle C \rangle = \alpha_C N H d^3 C_*(d), \qquad \alpha_C = \frac{\alpha\alpha_\gamma}{4\pi}, \tag{11.6}$$

see (7.13) and (10.2), and $\overline{\eta}_{in} \sim \overline{\eta}_{out}$ to be equal to the mean buoyancy averaged horizontally over a local Rossby radius and vertically over the mixing depth, so that

$$\overline{\eta} = \frac{\mathscr{D}}{\pi (N/f)^2 h^3} = \frac{\alpha_\gamma}{\pi} N^2 h, \tag{11.7}$$

equation (11.5) reduces to the algebraic transcendental equation

$$d^5 C_*(d) = \alpha_{Ri} Ri^{-3/2}, \qquad \alpha_{Ri} = \frac{\alpha\alpha_\gamma^2}{2\pi^2}. \tag{11.8}$$

Here, $d = h/H$ is the non-dimensional mixing depth defined in the previous sections, α_{Ri} is a new constant, and Ri is a new non-dimensional parameter, the bulk Richardson number

$$Ri = \frac{N^2 H^2}{(B_0 L_{hor})^{2/3}}, \tag{11.9}$$

where $L_{hor} = R_{out} - R_{in}$ is the horizontal lengthscale.

The solution of the equation $d = d_{eq}(Ri)$ defines the equilibrium mixing depth $d_{eq} < 1$ in terms of the Richardson number. Since Ri is independent of rotation, the mixing depth d_{eq} is also independent of rotation.

For $d \ll 1$, the speed of three-dimensional hetons is $C_*(d) \approx 0.75 d^{-2}$, see (7.11), the numerically calculated α has the value $\alpha = 0.25$ (following our numerical calculations this asymptotic holds even for $0 < d < 0.8$), and the solution of (11.8) is given by

$$d_{eq} = \alpha_d Ri^{-1/2}, \qquad \alpha_d = \frac{4.72}{\alpha_\gamma^{2/3}}. \tag{11.10}$$

Equation (11.10) shows that $h_{eq} = d_{eq} H$ is independent of H, and can be represented by the algebraic relation $h_{eq} = 4.72 \alpha_\gamma^{-2/3} (L_{hor} B_0)^{1/3} N^{-1}$. A similar scaling for the equilibrium mixing depth h_{eq} (for $R_{in} = 0$) follows from the arguments based on linear baroclinic instability theory applied to baroclinic waves at the edge of a plume population, as suggested and verified in experiments by Whitehead *et al.*

(1996). Thus, using the data from Whitehead *et al.* (1996) for the mixing depth $h_{eq} = 4.6(R_{out}B_0)^{1/3}N^{-1}$, our three-dimensional heton model can be calibrated to laboratory experiments. The value 4.6 is the upper bound of the values 3.9 ± 0.9 suggested by Visbeck *et al.* (1997). The calibration to these data sets gives

$$\alpha_\gamma = 1.33 \pm 0.38. \tag{11.11}$$

Using these α_γ in (7.13) and (11.10), we can calculate the mean velocity $\langle C \rangle$ of the heton spreading as

$$\langle C \rangle = \alpha'_C (L_{hor} B_0)^{1/3}, \qquad \alpha'_C = 0.077 \pm 0.022. \tag{11.12}$$

Finally, using this equation and (10.2) we obtain

$$\langle R(t) \rangle = \alpha'_C ((R_{out} - R_{in})B_0)^{1/3}\, t, \quad \alpha'_C = 0.077 \pm 0.022 \tag{11.13}$$

the linear spreading law for flows characterized by compensated potential vorticity anomalies.

Taking $d = d_{eq}(Ri) = 1$ in (11.8), we find the critical Richardson number Ri_{cr} for convection to penetrate down to the bottom

$$Ri_{cr} = \left(\frac{\alpha_{Ri}}{C_*(1)} \right)^{2/3}. \tag{11.14}$$

Estimating $C_*(1)$ as $C_{max}(1) = 0.8$, see (5.10), taking $\alpha = 0.25$ from our numerical experiments and the mean α_γ from (11.11), we obtain

$$Ri_{cr} = 0.67. \tag{11.15}$$

The critical Richardson number estimates the lower bound for the spreading law (11.13) to hold.

12. Parameterization of vortex-dominated lateral heat/buoyancy transport

The spreading law is important in oceanography since it allows us to estimate the lateral heat/buoyancy transport associated with deep-ocean convection events. In non-eddy-resolving ocean circulation models, this transport is usually parameterized by downgradient diffusion (see the recent discussions by Visbeck *et al.* 1997; Olbers *et al.* 2000). In models using a constant coefficient of diffusion, spreading of the mean radius of a localized convective region obeys a square-root law $\langle R \rangle \sim t^{1/2}$, and an even slower power law dependence $\langle R \rangle \sim t^{1/3}$ follows in the case when the coefficient of diffusion is proportional to a gradient of potential density. Our theory and the numerical experiments clearly show the existence of a linear power law $\langle R \rangle \sim t$ if nonlinear heton dynamics dominate the spreading, see §§ 8–10. This implies that commonly used diffusion-like parameterizations for lateral heat transport are questionable under conditions when the spreading is due to hetons. A much stronger linear law can lead to a more efficient lateral heat and mass flux at large time.

From the general point of view of heat and passive scalar transport theory (Isichenko 1992), the linear law of spreading gives an upper 'advective' bound for superdiffusion, and indicates that the statistics of geophysical fields associated with the spreading phenomenon should be essentially non-Gaussian. Commonly used downgradient diffusion parameterizations of lateral buoyancy transport implicitly rely on the assumption of quasi-Gaussian statistics of geophysical fields. In the framework of the nonlinear dynamical system of three-dimensional hetons, quasi-Gaussian behaviour can be expected only when phase trajectories of hetons continuously cover

some domain in phase space. It is obviously not the case for the splitting regimes of heton dynamics owing to the ballistic infinite character of the phase trajectories of hetons which do not interact with each other at large time (see §§ 6 and 8).

Although we have quantified the advective-type spreading in terms of 'microscopic' heton dynamics, the question remains how this spreading can be quantified on a 'macroscopic' level of description in terms of the mean fields of the flow. This is the problem of the parameterization of the heat flux. We have already made the first step towards the parameterization of the heat/buoyancy transport in the previous section. Indeed, we have estimated the heat flux for the spreading regime of motion using (11.4). In the form

$$J = c_e \langle V \rangle \langle \eta \rangle \tag{12.1}$$

it gives the scaling for the parameterization of the buoyancy flux, if the so called exchange coefficient

$$c_e = \frac{\langle C \rangle}{\langle V \rangle} \tag{12.2}$$

can be proved to be a slowly varying function for the region of parameters under consideration. Here, $\langle V \rangle$ is the characteristic mean flow velocity. In the framework of our theory, the characteristic flow velocity represents the integral effect of the population of hetons. For that reason, $\langle V \rangle$ has the same scaling upon d and γ as $\langle C \rangle$. So we can expect c_e to be approximately constant.

Referring to laboratory experiments, we can take the characteristic horizontal velocity of the mean flow induced by localized convection as twice the maximum swirling velocity V of vortices, found to be $V = 0.9\,(L_{hor} B_0)^{1/3}$ in experiments of Whitehead *et al.* (1996), and $V = 1.0\,(L_{hor} B_0)^{1/3}$ in experiments of Narimousa (1998). The factor two is due to the cyclonic velocity of the upper vortices and anticyclonic circulation of the lower vortices, see Narimousa (1998). Using $\langle C \rangle$ estimated by (11.12), we find $c_e = 0.043 \pm 0.07$ which is in the range estimated by Spall & Chapman (1998). Spall & Chapman (1998) discussed the universality of c_e, performing a comparison for all data which is available from laboratory and numerical experiments (on the localized deep-to-shallow convection and narrow fronts) and concluded that c_e is a slowly varying function for a wide range of the external parameters if spreading is dominated by heton-like vortices.

We stress that the quantification of the exchange coefficient c_e by (12.2) and (11.12) is also one of the results of our nonlinear three-dimensional heton theory. Recently, Visbeck *et al.* (1997) developed a parameterization scheme (NEW) based on the Green–Stone diffusive-type approach and the advective-type approach by Gent & McWilliams (1990) implemented through a skew diffusion coefficient. They found the ability of the NEW parameterization scheme to reproduce the equlibration of the localized convection regions (chimneys in the ocean) computed by realistic three-dimensional models. It would be interesting to compare the spreading laws resulting from the NEW parameterization and the corresponding spreading rate with those found by us using a quasi-geostrophic three-dimensional heton approach.

To summarize, when developing parameterizations for lateral heat/buoyancy fluxes, it is necessary to distinguish between balanced and non-balanced PV distributions. The distributions are balanced if they are created by heat sources (the case of convection), and they are non-balanced if they are created by, for example, wind stress. The influence of friction also can destroy the balance between cyclonic and anticyclonic PV in real oceanic conditions. However, at least in open-ocean deep convection (if it does not penetrate to the bottom) the PV balance should hold

(the case of shallow rotating convection needs more careful consideration). Moreover, spreading and confinement regimes of motion should be distinguished. The advective-type parameterization of the heat/buoyancy flux is valid only for spreading regimes.

13. Discussion

We discuss to what extent our results, in particular the linear spreading law, are universal, i.e. independent of the profile of heat release by the population of plumes, the specific profile of vertical stratification, boundary conditions at bottom and surface, and the geometry of the cooling region. The three-dimensional heton approximation simplifies the phenomenon of lateral spreading because it does not take into account ageostrophic effects due to vertical mixing and the radiation of superinertial waves. Moreover, in real convection, the Brunt–Väisälä frequency in the convective patch differs from ambient values. In the quasi-geostrophic approximation, this difference is entirely attributed to the action of the heat source on the right-hand side of the PV equation, and the action of this source leads to the creation of hetons. Since a buoyancy anomaly is associated with each heton, mean (area-averaged) stratification within the area where hetons are present differs from that of the ambient fluid. In the real world, we should recognize that this difference can be of the order of the background stratification within the convective patch, and, strictly speaking, we may find ourselves beyond the limits of applicability of the QG approximation. Thus, the QG approximation is a compromise, typical for the recent treatment of nonlinear vortex dynamics in localized convection (Legg & Marshall 1993; Legg *et al.* 1996; Visbeck *et al.* 1997; Danilov *et al.* 1998; Marshall & Schott 1999), which allows us to emphasize the nonlinear vortex-dominated mechanism of lateral spreading and to treat the dynamics of convective patches both by analytical means and by simple numerical simulations. We will discuss further several other issues: the differences between three-dimensional heton models and other heton models, the region of applicability of our results and the perspectives of the three-dimensional heton description in other problems of geophysical fluid dynamics.

13.1. *Universality of the linear spreading law*

We have shown that the spreading law of vortex-dominated lateral spreading from a localized convective region depends on the vertical structure of the PV field of localized vortices generated during the convection development. Only the compensated PV vortex structures – three-dimensional hetons – result in an advective-type lateral spreading of localized buoyancy anomaly associated with localized convection (see the PV constraint (2.20)). Indeed, in the case when the total PV of the two baroclinic vortices forming a heton is zero, the hetons have the property of self-propagation, see § 5, their trajectories of absolute motion are unbounded and their motion is along straight lines for $t \to \infty$ (see §§ 6 and 8). If the total PV of the two vortices is not compensated, the trajectories are finite and the vortices rotate around the centre of vorticity, the curvature of the trajectories being a function of the total PV remainder, see § 8 and Gryanik (1983*b*), Hogg and Stommel (1985*a*). We have shown, see § 2, that the vertically homogeneous distribution of heat released by plumes at the initial non-hydrostatic stage of vertical mixing is accompanied by the generation of positive and negative PV anomalies at the surface and at the bottom of the mixing layer. In turn, the assumption of vertical homogeneity naturally follows from the assumption that the heat flux decays linearly with depth inside the convective region (see Raasch & Etling 1998; Mironov *et al.* 2000). The linear dependence of the heat flux on z

is not just one of the possibilities, it is the basic property of statistically stationary turbulent convection forced at a constant rate (Raasch & Etling 1991, 1998). Thus, the existence of localized PV at the surface and the bottom of the mixing layer which form compensated PV vortex structures is a natural basic property of convection dominated by rotation (compare Jones & Marshall (1993), and Marshall & Schott (1999) who also discussed the property of PV balance for turbulent convective flows). It is worth mentioning that the balance of PV for the most unstable baroclinic mode developing at the edge of localized convective regions defines the success of the linear baroclinic instability theory (Pedlosky 1985; Kozlov *et al.* 1986) in the treatment of the lateral heat transport from localized convective regions (Jones & Marshall 1993; Visbeck *et al.* 1997), although the linear baroclinic instability theory cannot predict the detachment of vortices, the temporal development of the size of the baroclinic zone, and the self-propagation of vortices out of the localized convective region.

We have shown that if the vertical structure of PV is given and if zero PV, momentum and angular momentum constraints are satisfied, all dynamical aspects in the three-dimensional heton theory are defined by the Hamiltonian of interaction between vortices. The extent of universality of the regimes of motion and of the spreading law is determined by the universality of the Hamiltonian. The exact structure of the Hamiltonian for the case of an arbitrary stratification of the ambient fluid is defined by the corresponding Green function $G(r, z;\ r_0, z_0)$, see equations (4.18) and (4.3). The structure of Green's function depends on the profile of the Brunt–Väisälä frequency and also on the boundary conditions. The asymptotic behaviour of Green's function is universal at both small and large scales. At small scales ($r \ll L$), the stratification can always be approximated by a profile with constant Brunt–Väisälä frequency and therefore Green's function is algebraic, see (4.3) and (4.5). At large scales ($r \gg L$), Green's function has a universal barotropic (logarithmic) behaviour and thus is insensitive to the details of the stratification profile, see (4.4) and (4.6). Hence, it follows that the dependence of speed of three-dimensional hetons on the distance between vortices is always non-monotonic and universal at small ($C \sim b$) and large ($C \sim b^{-1}$) scales with some non-universal maximum at local Rossby radius scale. In the case where local and bulk Rossby radii are strongly different ($h \ll H$), there exists another universal asymptotic behaviour for Green's function if $L_h \ll r \ll L$. In this region, the influence of the lower boundary is not important and Green's function decays according to the three-dimensional law, see (4.5). For the speed of a heton we obtain $C \sim b^{-2}$. The rigid-lid boundary condition, used in our investigation, is natural at the bottom, and quite realistic at the upper boundary. When imposing it at the upper boundary we filter out the effect of superinertial waves. The procedure is well grounded if the typical size of the domain under consideration is much smaller than the external (barotropic) Rossby radius $L_0 = (gH)^{1/2}/f$. The three-dimensional heton dynamics become different only at scales comparable with or larger than the barotropic Rossby radius L_0, mainly because of the modification of the barotropic part of Green's function. For the real ocean, L_0 is much bigger than the bulk Rossby radius L which defines the typical scale for baroclinic vortices. Thus, the dynamics of hetons remain universal at all horizontal scales under consideration if the rigid-lid boundary conditions are used. For the atmosphere, the rigid lid condition is indeed too restrictive, as discussed in § 1. In the case of a QG two-layer model with a finite L_0, the analysis shows (Gryanik 1983*a*) that the speed of propagation of hetons exponentially decreases if $b \gg L_0$. The same is true here for a stratified fluid of finite depth in the light of the already mentioned analogy between the two-layer model and the two-mode approach at scales $b > \lambda_1^{-1}$.

The effect of the geometry of the cooling region on the lateral spreading was not analysed in our investigation in detail, but the analysis based on the kinetic equation in collisionless approximation shows that the linear spreading law is valid for regions with finite support in space in the limit of large time. The linear law of lateral spreading remains valid also for a strip-shaped geometry of the cooling region, as was shown in simulations with a two-layer heton model by Danilov *et al.* (2000).

These points indicate that the typical regimes of motion – the splitting and confinement regimes – and the phenomenon of lateral buoyancy spreading which is quantified by a linear spreading law of the mean radius of the localized buoyancy anomaly is quite robust and does depend only in detail on the history of the heat release by the population of plumes, the inhomogeneous background stratification, the boundary conditions at the bottom and the surface, and the geometry of the cooling region.

13.2. *Three-dimensional heton theory and other heton theories*

Conceptually, a similar model of hetons was suggested by Legg & Marshall (1993) for modelling the lateral spreading of a chimney in deep-ocean convection events. In their model, they assumed that the cyclonic PV is localized in an infinitely shallow layer just under the surface and that the anticyclonic PV is distributed over the whole volume of the mixed fluid layer. Notice that this is consistent with the quasigeostrophic PV equations ((2.1)–(2.5)) if it is assumed that the heat source $\mathcal{Q}$, but not the heat flux B (see discussion in the previous subsection), decays linearly down to the mixing depth. However, in Legg & Marshall's heton model, this asymmetry is eliminated by passing to a two-layer approximation with equal fluid-layer depths. Our analysis shows that the asymmetry in the vertical distribution of PV even under the condition of full compensation essentially influences both the structure of the velocity field of three-dimensional hetons and their dynamics, see for example the non-radial splitting in figures 7(*a*), 7(*b*) (§ 6) and in figure 10(*d*) (§ 7). This effect could be seen most clearly at scales $r \leqslant (N/f)h$. As follows from the structure of Green's function (see (4.3)), the surface charge of PV is in this case equivalent to a doubled volume charge owing to the summation with the image charge. At scales $r \gg (N/f)h$, this asymmetry is not seen because contributions from all image charges with respect to upper and lower boundaries become the same. Therefore, the model suggested by Legg & Marshall (1993), see also Gryanik (1983*a*) and Hogg & Stommel (1985*a*), can be used only if the heton evolution occurs at such scales. However, the comparison of the two-layer model with the three-dimensional heton model shows, see § 6, that a two-layer approximation with equal fluid-layer depths overestimates the splitting regimes of the heton dynamics. This is because the two-layer approximation is equivalent to a two-mode (barotropic and first baroclinic) approximation of the three-dimensional model, and this approximation neglects the vortex interaction due to the other baroclinic modes, which becomes important at small distances b. Moreover, in a two-layer model the heton propagation speed is $C \sim b \ln b$ for $b \leqslant (N/f)h$, as was shown by Gryanik (1983*a*), since the potential vorticity associated with a single vortex in the two-layer model is of finite vertical extent within the layers. Thus, the two-layer model overestimates the spreading rate of the heton population in comparison with the three-dimensional model ($C \sim b$ for $b \leqslant (N/f)h$, see § 5). Legg *et al.* (1996) paid attention to the overestimation of the lateral heat transport by two-layer heton models in comparison with results from numerical experiments with LES models, but this overestimation was attributed to the inability of the heton model to simulate the growth of the Rossby radius with time owing to the growing of the mixing depth with time. Here, we have argued that this overestimation can be explained

also by the restrictive approximation of the two-layer heton model itself. Moreover, it is also necessary to bear in mind that, as shown by Dritschel & Juárez (1996), the columnar vortex pairs in a continuously stratified QG fluid are unstable to three-dimensional perturbations when the vortex height-to-width aspect ratio exceeds approximately $3(f/N)$. This instability results in localized quasi-ellipsoidal baroclinic vortices at the lower and the upper surfaces. In the laboratory experiments with continuously stratified fluids, quasi-ellipsoidal rather than column-like localization of baroclinic vortices was documented (Narimousa 1998; Boubnov & Rhines 1999, private communication). Obviously, the structure and long-time dynamics of the quasi-ellipsoidal localized vortices can be better modelled in the first approximation by three-dimensional point vortices.

Generally speaking, the two-layer model by Legg & Marshall (1993) – where PV anomalies of opposite signs are distributed uniformly within respective layers – and the three-dimensional model suggested in this paper – where PV anomalies are distributed only at two levels – are complementary cases which correspond to different limiting cases of vertical PV distribution. The exact structures of both vertical and horizontal PV distributions associated with turbulent convection dominated by rotation still call for further investigations. In particular, if we discuss the estimation of the spreading rate of the localized convective region and the applicability of quasi-geostrophic models of point vortices for that estimation, the most important issues that should be addressed are the vertical distribution of quasi-geostrophic PV and the horizontal intermittency of the PV field, at times exceeding that of geostrophic adjustment. Data from large-eddy simulations are expected to be an effective aid in pursuing this line of research. Only then may we judge which model is preferable. In any case, the three-dimensional heton model is more general than two-layer (Gryanik 1983*a*; Hogg & Stommel 1985*a*, *b*; Legg & Marshall 1993; Danilov *et al.* 2000) and multi-layer models (Gryanik & Tevs 1989, 1997), since it allows us to approximate more general vertical distributions of PV by properly adjusting the positions of vortices, and since it incorporates more physics at scales smaller than the bulk Rossby radius in comparison with the two-layer counterpart.

13.3. *Limit of the three-dimensional heton idealization*

Several limitations of the developed QG three-dimensional point heton theory and other point heton theories are also obvious. The theories do not take into account the finite size of PV anomalies. The point heton idealization presents an external asymptotic of the geophysical fields for compact distributions of potential vorticity. Several procedures of regularization are known (see e.g. Goncharov & Gryanik 1986; Sutyrin, McWilliams & Saravanan 1998), and all of them show that the point-vortex approximation is the leading-order expansion for geophysical fields in the small parameter which is the ratio between the PV anomaly core-size and the separation between vortices. However, the effects of stability of the finite-core hetons are not investigated in this paper, but it should be born in mind that such effects may be important for heton cluster formation, and, thus, for the rate of spreading. In particular, the model does not take into account merging events (Verron & Valcke 1994; Sokolovskiy & Verron 2000) associated with the finite size of PV anomalies and dissipation, which result in an increase of the size of baroclinic vortices. The phenomenon of temporal increase of the size of baroclinic vortices during the convection development under long-time forcing was observed in both laboratory, e.g. Ivey *et al.* (1995) and Whitehead *et al.* (1996), and numerical experiments, e.g. Legg *et al.* (1996), but it was attributed to the growth of the local Rossby radius

$L = (N/f)h$ in time owing to the growth of the mixing-layer depth h. To what extent the combined effect of merging of baroclinic vortices, and temporal growth of the local Rossby radius is able to modify the linear spreading law is an open question. While the effect of dissipation, e.g. through the merging mechanism, on three-dimensional heton dynamics can be important at the stage of heton formation it is insignificant at the spreading stage of evolution of individual tilted hetons because the characteristic time of viscous dissipation at that stage is much larger than the characteristic time of the lateral spreading process.

We notice also that the available potential energy of the buoyancy anomaly is converted into the energy of the hetons or clusters of hetons (propagating out of the convective patch), the energy of the radiated superinertial waves and the energy of small-scale turbulent motions (Sander *et al.* 1995; Hermann & Owens 1993). The QG three-dimensional heton description takes into account only the transfer of potential energy into the heton kinetic and potential energies and neglects the transfer of energy into small-scale turbulence and the superinertial waves. Each propagating heton contains both kinetic and potential energy, see Appendix B and compare Gryanik & Tevs (1997). The ratio of kinetic to potential energy for a single heton depends essentially on the heton size b, as has been shown in Gryanik & Tevs (1997) for hetons in a multi-layer model. In particular, this ratio goes to zero when $b \to 0$. Moreover, the propagation of heton clusters is accompanied by a temporal conversion of potential to kinetic energy and vice versa owing to periodical oscillations of their sizes during the motion, see trajectories of heton clusters in figures 12 and 17. Some conclusions about the effects of energy loss due to radiation of superinertial waves on the spreading process can be drawn from the analysis of the evolution of an individual heton using adiabatic perturbation theory (Goncharov & Gryanik 1986; Gryanik 1992). Indeed, superinertial waves do not carry PV out of the region of generation, so we can assume $\delta\gamma = 0$. For that case, the variation of the Hamiltonian (7.1), being the variation of energy (see Appendix B) is

$$\delta\mathscr{H} = \frac{\mathrm{d}}{\mathrm{d}b}G(b, 0, -h)\delta b < 0. \tag{13.1}$$

From (4.3), we have $\delta G(b, 0, -h)/\delta b > 0$ and from (13.1), it follows that $\delta b < 0$. So, the heton will accelerate for $b > b_{max}$ and slow down for $b < b_{max}$, as can be seen from (5.4), (5.5) and figure 4. Since, for the spreading regimes of heton motion, we have predominantly $0 < b < b_{max}$ (see § 6.3), the radiation of superinertial waves results in a reduction of the spreading rate. The effect of acceleration of a heton for $b > b_{max}$ and deceleration for $b < b_{max}$ owing to radiation of superinertial waves, is similar to the corresponding effect owing to radiation of Rossby waves (Gryanik 1992); however, the estimation of the magnitude of deceleration due to radiation of superinertial waves (unlike Rossby waves), is outside the region of validity of the QG approximation used in our theory.

13.4. *Perspectives of the three-dimensional heton idealization and future work*

The analysis of scenarios of lateral spreading of localized buoyancy anomalies owing to heton-like vortex structures, performed in this paper was limited to the case of an initially quiescent fluid. Under real geophysical conditions in the ocean, the lateral spreading proceeds on a background of barotropic and baroclinic shear flows and mesoscale cyclonic and anticyclonic eddies. Recently, Legg & Marshall (1998) investigated the influence of an axisymmertic cyclonic vortical flow on the lateral spreading using the two-layer QG heton model. They have found a suppression of

the splitting regimes of heton motion by a vortical flow, but have not quantified the spreading law. An additional suppression of spreading can result from the deviation of the vertical PV distribution from a balanced one, which can arise, for example, through a vertical asymmetry of the dissipation owing to the boundary layers. The interaction with background baroclinic and barotropic shear flows may result in an horizontal asymmetry of lateral spreading owing to a suppression of spreading in the crossflow direction. In this case, the general three-dimensional heton model, see § 3, which is able to describe the interaction of three-dimensional hetons with background flows and non-balanced vertical PV distributions should be used. Some insight into the problem is gained in the analytical studies of e.g. Doronina (1995); Walsh & Pratt (1995); and Gryanik & Doronina (1997) in which the mechanism of interaction of a localized baroclinic vortex of non-balanced PV distribution with constant background vertical shear flows (Doronina 1995; Walsh & Pratt 1995) and with both vertical and horizontal constant shear flows (Gryanik & Doronina 1997) were analysed. Extension of these investigations to the effect of heat forcing is required to quantify the spreading laws of localized buoyancy anomalies in real geophysical conditions in the ocean. The case of lateral vortex-dominated spreading in localized convection over a sloping bottom (topographic β-effect) is also of importance in oceanographic investigations (see, e.g. Gawarkiewicz & Chapman 1995). Obviously the topographic β-effect results in an asymmetric lateral spreading of buoyancy anomalies created by convection. For small slopes (QG approximation is to be used) the analysis of heat/buoyancy transport by β-plane three-dimensional hetons (Flierl 1987; Gryanik 1988) can give some insight into the complex problem of asymmetric transport. Quantification of the spreading law for that case is a subject for future research. To what extent the effect of acceleration of a heton for $b > b_{max}$ and deceleration for $b < b_{max}$ owing to radiation of topographic Rossby waves, which can be estimated using the analysis of Rossby wave radiation by a heton (Gryanik 1988), will control the spreading is also an open question.

The problem of quantifying the spreading law for situations of a highly correlated heton-like dynamics which coexist with a chaotic dynamics of a sea of individual vortices (typical for confinement regimes of motion) was outside our investigation. The spreading law for these conditions remains to be analysed. For that case, we expect the superdiffusion spreading law to hold, but additional work is necessary to prove or to reject our suggestion. Additional work is also necessary to quantify the spreading law for the more general case of convection events characterized by unbalanced PV distributions, e.g. convection in shear flows, where we expect, as already was mentioned above, a substantial reduction of spreading.

Finally, the QG heton theory proved to be a reasonable idealized description which focuses study on the vortex-dominated mechanism of the lateral spreading of localized buoyancy anomalies created in continuously stratified rotating fluids of finite depth. Such anomalies can be created in the real ocean and atmosphere not only by localized convection. Other examples are the buoyancy anomaly of a narrow straight-line front in the ocean (see e.g. Spall & Chapman 1998), considered in connection with the problem of oceanic mesoscale heat/buoyancy mixing, and the buoyancy anomalies in the atmosphere at the interface between the troposphere and stratosphere (Juckes 1994), considered in connection with studies concerning the hypothesis of PV homogenization in the troposphere. A particular case is quasi-geostrophic surface buoyancy/temperature anomalies (Held *et al.* 1995). The knowledge of the structure and dynamics of the mutual interaction between three-dimensional hetons can be used to treat the above-mentioned problems also, because the basic three-dimensional heton

model, see § 3, can be adapted easily to the case of more realistic stratifications (profiles of the Brunt–Väisälä frequency $N(z)$) and boundary conditions (not necessarily a rigid lid at the surface and at the bottom) by the use of the appropriate Green function. Horizontal and vertical inhomogeneities of buoyancy anomalies can be modelled by the choice of appropriate horizontal and vertical PV distributions.

We should also mention that from the general point of view of dynamical systems theory, the quasi-geostophic three-dimensional point heton model gives us an example of a two-dimensional Hamiltonian dynamical system (see § 3) which incorporates the effect of the third dimension implicitly through the parameter of the vertical position of the vortices. The dynamics of vortices in our three-dimensional heton model can be investigated by Hamiltonian methods which were well developed for point vortex models in two-dimensional hydrodynamics (see, e.g. Eckhardt & Aref 1988). The close analogy between two-dimensional vortex dynamics and dynamics of quasi-geostrophic surface buoyancy/temperature anomalies emphasized in the theory of linear instability and quasi-geostrophic turbulence (Held *et al.* 1995), is expanded by our three-dimensional heton Hamiltonian description for the case of nonlinear localized perturbations. We hope also that our three-dimensional heton model will be useful for other problems of geophysical fluid dynamics in which the flow is dominated by the dynamics of heton-like vortex structures, e.g. the treatment of passive scalar transport due to localized heton-like vortices (cf. Doronina 1995).

14. Summary

In this paper, we have considered the problem of lateral heat/buoyancy transport in localized turbulent convection in continuously stratified fluids of finite depth dominated by rotation, which is characterized by strong horizontal intermittency due to the self-organization of the flow into populations of isolated coherent vortices. We have focused our investigation on the physical mechanism of vortex-dominated lateral spreading of anomalous buoyancy created by localized convection at fast rotation rate (typical for geophysical conditions in the ocean and atmosphere) and quantified the spreading law in terms of both internal (specific for vortex dynamics) and external (specific for convection) parameters. The quantification was performed both analytically and numerically by developing a three-dimensional point heton theory which presents a physically motivated idealized description (formulated in terms of potential vorticity evolution) for the lateral heat/bouyacy redistribution which is due to outward propagating intense heton-like vortices appearing in the convective region, each carrying a portion of buoyancy anomaly.

We have shown by the analysis of the particular properties of the three-dimensional-heton structure and dynamics, that there are two fundamental dynamical regimes of evolution for localized buoyancy anomalies. These are the splitting and confinement regime. We have found that if the splitting regime is realized, the mean radius of a localized region $\langle R \rangle$ and its variance σ grow linearly with time, $\langle R \rangle \sim t$ and $\sigma \sim t$. We have shown that the necessary conditions for the advective-type spreading law to hold are zero PV, momentum and angular momentum constraints, which is a natural property of convection generated by localized heat sources in an initially quiescent fluid. A theoretical explanation for the spreading law has been given in terms of the asymptotic dynamics of a single heton and within the frames of the kinetic equation derived for the distribution function of hetons in collisionless approximation.

By our theoretical analysis and numerical experiments, we have found a mixing-depth-dependent scaling for the three-dimensional heton spreading rate. The spreading

rate $\langle C \rangle$ scales with the mean speed of propagation of individual hetons or heton clusters and is proportional to the strength of hetons γ and inversely proportional to the square of the ratio of local to bulk Rossby radii. In terms of the external convective parameters the spreading rate is $\langle C \rangle = \alpha_C (L_{hor} B_0)^{1/3}$, where $\alpha'_C = 0.077 \pm 0.022$.

We have concluded that the linear law of buoyancy spreading implies that a down-gradient diffusion parameterization of lateral buoyancy transport is not appropriate for the case when the splitting regime of heton dynamics dominates, and the zero PV, momentum and angular momentum constraints are satisfied. For that case, we will suggest an advective-type parameterization, which can be treated also as skew diffusion (cf. Moffatt 1983; Gent & McWilliams 1990). We have shown that our three-dimensional heton theory gives an estimation of the heat/buoyancy flux, suggests the scaling for the parameterization of this flux, and quantifies the exchange coefficient c_e in terms of the mean propagation speed of hetons. The development of the parameterization itself for the case of balanced PV distributions, and its detailed comparison with the Gent & McWilliams (1990) parameterization and the other approaches, is the subject of a forthcoming paper.

Finally, in this paper we have also discussed the region of applicability of our results, the perspectives of the three-dimensional heton description in problems of localized convection of complex oceanic flows, and have outlined some other problems of geophysical fluid dynamics (the mesoscale lateral eddy-transport in the ocean, the PV homogenization in the troposphere, the surface quasi-geostrophic dynamics, and the passive scalar transport from localized convective regions) in which the evolution of flows is dominated by the dynamics of heton-like vortex structures and heton theories can be applied.

V. G. and T. D. are very grateful to B. Boubnov, who in discussions over many years generously shared with them his deep knowledge of turbulent convection dominated by rotation. We are glad to thank H. Borth, S. Danilov, B. Eckhardt, G. Golitsyn, R. Käse, V. Lykossov, D. Mironov, J. Sander, M. Sokolovskiy, C. Völker and A. Yaremchuk for fruitful discussions. The authors thank four official reviewers for their very helpful comments. The work was supported by Volkswagen Stiftung under grant I/71 611 and by EC project CARTUM – Contract MAS3-CT98-0172.

This work is Contribution Number 1397 of the Alfred-Wegener-Institute for Polar and Marine Research.

Appendix A. Green's function

The connection between the two expressions for Green's function given by equations (4.3) and (4.5) can be established in a few steps. First, we calculate the Fourier transform $G(\boldsymbol{k}, k_z)$ of (4.3):

$$G(\boldsymbol{k}, k_z) = \frac{\mathrm{e}^{\mathrm{i}\boldsymbol{k}\boldsymbol{r}_0 + \mathrm{i}k_z z_0}}{\boldsymbol{k}^2 + \boldsymbol{k}_0^2} \sum_{m=-\infty}^{\infty} \mathrm{e}^{2\mathrm{i}kHm}. \tag{A 1}$$

where $\boldsymbol{k}$ and k_z are the horizontal and vertical wavenumbers respectively. Secondly, we use the Poisson summation formula which gives

$$\sum_{m=-\infty}^{\infty} \mathrm{e}^{2\mathrm{i}kHm} = 4\pi \sum_{n=-\infty}^{\infty} \delta(Hk - \pi n). \tag{A 2}$$

Finally, the inverse Fourier transform of (A 1) gives equation (4.5).

Green's function shows the influence of an individual point vortex in the model. This influence can be made clear through the consideration of the short- and long-range asymptotics of Green's function. The short-range behaviour, $r^2 + (N^2/f^2)z^2 \ll (N^2/f^2)H^2$ can be found from equation (4.4) which shows that the flow is essentially baroclinic in this limit. The long-range asymptotics ($r \to \infty$) follows from equation (4.6). The flow structure here is dominated by the first term at $r \gg (N/f)H$ which is independent of the vertical coordinate, i.e. a barotropization of the flow takes place. All other terms have exponential decay due to the exponential decay of the modified Bessel function $K_0(r) \sim r^{-1/2}\exp(-r)$ at $r \gg 1$.

Appendix B. Energetics

The total energy of a three-dimensional heton population is given by

$$\mathscr{E} = \mathscr{E}_0 + \mathscr{H}. \tag{B 1}$$

Here, $\mathscr{E}_0$ is the total self-energy of the hetons which is independent of time and $\mathscr{H}$ is the energy of mutual interaction. Each part of this consists of two parts, that is,

$$\mathscr{H} = \mathscr{A} + \mathscr{K} \tag{B 2}$$

where the available potential energy is defined by

$$\mathscr{A} = \frac{\rho_0 f^2}{2N^2} \int \left(\frac{\partial \Psi}{\partial z}\right)^2 \mathrm{d}x\,\mathrm{d}y\,\mathrm{d}z \tag{B 3}$$

and the kinetic energy by

$$\mathscr{K} = \tfrac{1}{2}\rho_0 \int (\nabla\Psi)^2 \,\mathrm{d}x\,\mathrm{d}y\,\mathrm{d}z. \tag{B 4}$$

The energy conservation law in the model is

$$\frac{\mathrm{d}}{\mathrm{d}t}\mathscr{E} = -\int \Psi S(x, y, z, t)\,\mathrm{d}x\,\mathrm{d}y\,\mathrm{d}z. \tag{B 5}$$

The Hamiltonian $\mathscr{H}$ can be calculated in a straightforward way

$$\mathscr{H} = -\tfrac{1}{2}\rho_0 \int Q\Psi \,\mathrm{d}x\,\mathrm{d}y\,\mathrm{d}z = -\tfrac{1}{2}\rho_0 \sum_{i=1}^{\mathscr{N}} \gamma_i \Psi\Big|_{r_i}. \tag{B 6}$$

The total momentum, and angular momentum

$$\mathscr{P}_\alpha = \rho_0 \varepsilon_{\alpha\beta} \int r_\beta Q \,\mathrm{d}x\,\mathrm{d}y\,\mathrm{d}z, \quad \mathscr{J} = \rho_0 \int r^2 Q \,\mathrm{d}x\,\mathrm{d}y\,\mathrm{d}z, \tag{B 7}$$

satisfy, respectively,

$$\frac{\mathrm{d}}{\mathrm{d}t}\mathscr{P}_\alpha = \rho_0 \varepsilon_{\alpha\beta} \int r_\beta S(x, y, z, t)\,\mathrm{d}x\,\mathrm{d}y\,\mathrm{d}z, \tag{B 8}$$

$$\frac{\mathrm{d}}{\mathrm{d}t}\mathscr{J} = \rho_0 \int r^2 S(x, y, z, t)\,\mathrm{d}x\,\mathrm{d}y\,\mathrm{d}z. \tag{B 9}$$

In our case, their explicit calculation is also straightforward:

$$\mathscr{P}_\alpha = \rho_0 \varepsilon_{\alpha\beta} \int r_\beta Q \,\mathrm{d}x\,\mathrm{d}y\,\mathrm{d}z = \rho_0 \sum_{i=1}^{\mathscr{N}} \gamma_i r_\beta\Big|_{r_i} = \rho_0 \sum_{i=1}^{\mathscr{N}} \gamma_i r_{\beta i}, \tag{B 10}$$

$$\mathscr{J} = \rho_0 \int r^2 Q \, \mathrm{d}x \, \mathrm{d}y \, \mathrm{d}z = \rho_0 \sum_{i=1}^{\mathscr{N}} \gamma_i r^2 \Big|_{r_i} = \rho_0 \sum_{i=1}^{\mathscr{N}} \gamma_i r_i^2. \tag{B 11}$$

Appendix C. Deficit of buoyancy of a three-dimensional heton

The total deficit of buoyancy associated with one vertically aligned three-dimensional heton is given by the integral

$$\mathscr{D} = \int_{-H}^{0} \eta \, \mathrm{d}z, \tag{C 1}$$

where $\eta = f(\partial \overline{\Psi}/\partial z)$ with the horizontally averaged stream function

$$\overline{\Psi} = 2\pi\gamma \int_0^{\infty} [G(r, z, 0) - G(r, z, -d)] r \, \mathrm{d}r. \tag{C 2}$$

We substitute Green's function in the form given by (4.5) into (C 2). Using the formula

$$\int_0^{\infty} K_n(\lambda_n r) r \, \mathrm{d}r = \frac{1}{\lambda_n^2}, \tag{C 3}$$

(see Gradshteyn & Ryzhik 1980), with $K_n(r)$ the modified Bessel function, and $\lambda_n = \pi n/L$, as well as the relation

$$\sum_{n=1}^{\infty} \frac{\cos(nz)}{n^2} = \tfrac{1}{6}\pi^2 - \tfrac{1}{2}\pi z + \tfrac{1}{4} z^2, \tag{C 4}$$

(see Gradshteyn & Ryzhik 1980), we obtain

$$\overline{\Psi}(z) = \frac{\gamma N^2}{f^2 H} \begin{cases} (z-h)H - \frac{1}{2}h^2 & (h < z < 0), \\ -\frac{1}{2}h^2 & (-H < z < h). \end{cases} \tag{C 5}$$

Finally, taking the derivative of (C 5), substituting the result into (C 1) and performing the elementary integration in z we obtain the buoyancy deficit

$$\mathscr{D} = \gamma \frac{N^2 h}{f}. \tag{C 6}$$

The buoyancy deficit $\mathscr{D}$ carried by a tilted three-dimensional heton remains the same as for a vertically aligned heton. The buoyancy deficit of the population of $\mathscr{N}$ three-dimensional hetons is $\mathscr{D}_{\mathscr{N}} = \mathscr{N}\mathscr{D}$. This fact can be understood by the property of linear superposition of contributions from point vortices forming hetons and heton populations.

Appendix D. Calculation of the function $\alpha(d)$

To estimate the mean propagation velocity $\langle C \rangle$, we substitute the distribution function given by (7.12) into (7.9). The result is

$$\langle C \rangle = \left[2\pi \int_0^{b_*} \left(\frac{C(x, d)}{\pi b_*^2} \right)^2 b \, \mathrm{d}b \right]^{1/2}. \tag{D 1}$$

Introducing the new variable $x = b/b_*$, it is easy to recognize that the propagation velocity $C_*(d)$ is the relevant velocity for scaling. After rearranging the terms, we obtain (7.13) and (7.14).

In the limit of infinite depth $d \ll 1$, the integral (7.14) can be calculated explicitly using the asymptotic limit (5.6) for the propagation speed C of the heton. Straightforward integration gives

$$\alpha = 2^{-1/2} c_*^2 (1 + c_*^2)^{1/2} \approx 0.69, \tag{D 2}$$

where $c_* \approx 0.86$ is given by (6.10). The analysis shows that the function $\alpha(d)$ slightly deviates from the limit of infinite depth (D 2) in the range $0.8 < d < 1$. Moreover, the analysis shows that the contribution to the integral (7.9) from $b \ll b_*$ is small and the basic contribution comes from $b \sim b_* \sim b_{max}$, owing to the linear behaviour of both the propagation speed C and the distribution function at small b.

REFERENCES

Boubnov, B. M. & Golitsyn, G. S. 1986 Experimental study of convective structures in rotating fluids. *J. Fluid Mech.* **167**, 503–531.

Boubnov, B. M. & Golitsyn, G. S. 1990 Temperature and velocity field regimes of convective motions in a rotating plane fluid layer. *J. Fluid Mech.* **219**, 215–239.

Boubnov, B. M. & Golitsyn, G. S. 1995 *Convection in Rotating Fluids.* Kluwer.

Brickman, D. 1995 Heat flux partitioning in deep-ocean convection. *J. Phys. Oceanogr.* **25**, 2609–2623.

Charney, J. G. 1963 Numerical experiments in atmospheric hydrodynamics. *Proc. Symp. in Appl. Math. Am. Math. Soc.* **15**, 289–310.

Danilov, S., Gryanik, V. & Olbers, D. 2000 Equilibration and lateral spreading of a strip-shaped convective region. *J. Phys. Oceanogr. accepted.* [Available from Alfred-Wegener-Institute für Polar-und Meeresforschung. 1998 AWI Rep. 86, 23 pp.]

Dikarev, S. N. 1983 On the influence of rotation on the convective structure in deep homogeneous fluid. *Dokl. Akad. Nauk SSSR* **273**, 718–720.

Doronina, T. N. 1995 Structure of circulation cells of intense baroclinic vortices in flows with velocity shear and advective admixture transfer. *Izv. Atmos. Ocean Phys.* **31**, 223–232.

Doronina, T. N. 1997 Interaction of baroclinic point vortices in quasi-geostrophic barotropic and baroclinic shear flows. *Oceanology.* **37**, 506–512.

Dritschel, D. G. & de la Torre Juárez, M. 1996 The instability and breakdown of tall columnal vortices in quasi-geostrophic fluid. *J. Fluid Mech.* **328**, 129–160.

Eckhardt, B. & Aref, H. 1988 Integrable and chaotic motions of four vortices II. Collision dynamics of vortex pairs. *Phil. Trans. R. Soc. Lond.* A **326**, 655–696.

Egger, J. 1992 Point vortices in a low-order model of barotropic flow on the sphere. *Q. J. R. Met. Soc.* **118**, 533–552.

Fernando, H. J. S., Chen, R. & Boyer, D. L. 1991 Effects of rotation on convective turbulence. *J. Fluid Mech.* **228**, 513–547.

Flierl, G. R. 1987 Isolated eddy models in geophysics. *Ann. Rev. Fluid Mech.* **19**, 493–530.

Gawarkiewicz, G. & Chapman, C. 1995 A numerical study of dense water formation and transport on a shallow, sloping continental shelf. *J. Geophys. Res.* **100** (C3), 4489–4507.

Gent, P. & McWilliams, J. 1990 Isopycnal mixing in ocean circulation models. *J. Phys. Oceanogr.* **20**, 150–155.

Goncharov, V. P. & Gryanik, V. M. 1986 Dynamics of solitary dissipative vortices: vortex lattices and their stability. *Sov. Phys. J. Exp. Theor. Phys.* **64**(5), 976–983.

Gradshteyn, I. S. & Ryzhik, I. M. 1980 *Table of Integrals, Series, and Products.* Academic.

Griffiths, R. W. & Hopfinger, E. J. 1986 Experiments with baroclinic vortex pairs in a rotating fluid. *J. Fluid Mech.* **173**, 501–518.

Gryanik, V. M. 1983*a* Dynamics of singular geostrophic vortices in a two-layer model of the atmosphere (ocean). *Izv. Atmos. Ocean Phys.* **19**, 171–179.

Gryanik, V. M. 1983*b* Dynamics of localized vortex perturbations 'vortex charges' in a baroclinic fluid. *Izv. Atmos. Ocean Phys.* **19**, 347–352.

Gryanik, V. M. 1988 Localized vortices – 'vortex charges' and 'vortex filaments' in a baroclinic differentially rotating fluid. *Izv. Atmos. Ocean Phys.* **24**, 919–926.

Gryanik,V. M. 1992 Radiation of Rossby waves and adaptation of potential vorticity fields in the atmosphere (ocean). *Trans. Dok. USSR Acad. Sci.* **326**, 976–979.

Gryanik, V. M. & Doronina, T. N. 1997 The interaction between intense baroclinic quasi-geostrophic vortices in flows with vertical and horizontal velocity shear. *Izv. Atmos. Ocean Phys.* **33**, 171–183.

Gryanik, V. M. & Tevs, T. N. 1989 Dynamics of singular geostrophic vortices in a N-layer model of the atmosphere (ocean). *Izv. Atmos. Ocean Phys.* **25**, 179–188.

Gryanik, V. M. & Tevs, M. V. 1997 Dynamics and energetics of heton interactions in linearly and exponentially stratified media. *Izv. Atmos. Ocean Phys.* **33**, 419–433.

Held, I. M., Pierrehumbert, R. T., Garner, S. T. & Swanson, K. L. 1995 Surface quasi-geostrophic dynamics. *J. Fluid Mech.* **282**, 1–20.

Helfrich, K. R. & Battisti, T. M. 1991 Experiments on baroclinic vortex shedding from hydro-thermal plumes. *J. Geophys. Res.* **96**, 12 511–12 518.

Hermann, A. J. & Owens, W. B. 1993 Energetics of gravitational adjustment for mesoscale chimneys. *J. Phys. Oceanogr.* **23**, 346–371.

Hogg, N. G. & Stommel, H. M. 1985*a* The heton, an elementary interaction between discrete baroclinic geostrophic vortices, and its implications concerning eddy heat-flow. *Proc. R. Soc. Lond.* A **397**, 1–20.

Hogg, N. G. & Stommel, H. M. 1985*b* Hetonic explosions: the breakup and spread of warm pools as explained by baroclinic point vortices. *J. Atmos. Phys.* **42**, 1465–1476.

Hopfinger, E. J. & van Heijst, G. J. F. 1993 Vortices in rotating fluids. *Ann. Rev. Fluid Mech.* **25**, 241–289.

Isichenko, M. B. 1992 Percolation, statistical topography, and transport in random media. *Rev. Mod. Phys.* **64**, 961–1043.

Ivey, G. N., Taylor, J. R. & Coates, M. J. 1995 Convectively driven mixed layer growth in a rotating, stratified fluid. *Deep-Sea Res.* **42**, 331–349.

Jones, H. & Marshall, J. 1993 Convection with rotation in a neutral ocean: a study of deep-ocean convection. *J. Phys. Oceanogr.* **23**, 1009–1039.

Juckes, M. 1994 Quasi-geostrophic dynamics of the tropopause. *J. Atmos. Sci.* **51**, 2756–2768.

Käse, R. H. 1998 Modeling of the oceanic mixed layer and effects of deep convection. In *Buoyant Convection in Geophysical Flow*. Kluwer.

Klinger, B. A. & Marshall, J. 1995 Regimes and scaling laws for rotating deep convection in the ocean. *Dyn. Atmos. Oceans.* **21**, 227–256.

Kozlov, V. F., Makarov, V. G. & Sokolovskiy, M. A. 1986 Numerical model of the baroclinic instability of axially symmetric eddies in two-layer ocean. *Izv. Atmos. Ocean Phys.* **22**, 674–678.

Legg, S., Jones, H. & Visbeck, M. 1996 A heton perspective of baroclinic eddy transfer in localized open ocean deep convection. *J. Phys. Oceanogr.* **26**, 2251–2266.

Legg, S. & Marshall, J. 1993 A heton model of the spreading stage of open-ocean deep convection. *J. Phys. Oceanogr.* **23**, 1040–1056.

Legg, S. & Marshall, J. 1998 The influence of the ambient flow on the spreading of convected water masses. *J. Mar. Res.* **56**, 107–139.

Lifshitz, E. M. & Pitaevsky, L. P. 1979 *Physical Kinetics.* Moscow. (In Russian).

Marshall, J. & Schott, F. 1999 Open-ocean convection: observations, theory and models. *Rev. Geophys.* **37**, 1–64.

Maxworthy, T. & Narimousa, S. 1994 Unsteady, turbulent convection into a homogeneous rotating fluid, with oceanographic applications. *J. Phys. Oceanogr.* **24**, 865–887.

Mironov, D. V., Gryanik, V. M., Moeng, C.-H., Olbers, D. & Warncke, T. H. 2000 Vertical turbulence structure and second-moment budgets in convection with rotation: a large-eddy simulation study. *Q. J. R. Met. Soc.* **126**, 477–515.

Moffatt, H. K. 1983 Transports effects associated with turbulence with particular attention to the influence of helicity. *Rep. Prog. Phys.* **46**, 621–664.

Narimousa, S. 1998 Turbulent convection into a linearly stratified fluid: the generation of 'subsurface anticyclones'. *J. Fluid Mech.* **354**, 101–121.

Olbers, D., Wolff, J.-O. & Völker, C. 2000 Eddy-fluxes and second order moment balances for non-homogeneous quasigeostrophic turbulence in wind-driven zonal flows. *J. Phys. Oceanogr.* **30**, 1645–1668.

Pedlosky, J. 1979 *Geophysical Fluid Dynamics.* Springer. 625 pp.

Pedlosky, J. 1985 The instability of continuous heton clouds. *J. Atmos. Sci.* **42**, 1477–1486.

Raasch, S. & Etling, D. 1991 Numerical simulation of rotating turbulent thermal convection. *Beitr. Z. Phys. Atmos.* **64**, 185–199.

Raasch, S. & Etling, D. 1998 Modelling deep ocean convection: large-eddy simulation in comparison with laboratory experiments. *J. Phys. Oceanogr.* **28**, 1786–1802.

Sander, J., Wolf-Gladrow, D. & Olbers, D. 1995 Numerical studies of open ocean deep convection. *J. Geophys. Res.* **100** (C10), 20 579–20 600.

Sokolovskiy, M. A. 1989 Head-on collisions of distributed hetons. *Trans. Dokl. USSR Acad. Sci.*, **306**, 215–217.

Sokolovskiy, M. A. & Verron, J. 2000 Finite-core hetons: stability and interactions. *J. Fluid Mech.* **423**, 127–154.

Spall, M. A. & Chapman, D. C. 1998 On the efficiency of baroclinic eddy heat transport across narrow fronts. *J. Phys. Oceanogr.* **28**, 2275–2287.

Straneo, F. & Kawase, M. 1999 Comparisons of localized convection due to localized forcing and to preconditioning. *J. Phys. Oceanogr.* **29**, 55–68.

Sutyrin, G. G., McWilliams, J. & Saravanan, R. 1998 Co-rotating stationary states and vertical alignment of geostrophic vortices with thin core. *J. Fluid Mech.* **357**, 321–349.

Verron, J. & Valcke, S. 1994 Scale-dependent merging of baroclinic vortices. *J. Fluid Mech.* **264**, 81–106.

Visbeck, M., Marshall, J., Haine, T. & Spall, M. 1997 Specification of eddy transfer coefficients in coarse-resolution oceans circulation models. *J. Phys. Oceanogr.* **27**, 381–402.

Walsh, D. & Pratt, L. J. 1995 The interaction of a pair of point potential vortices in uniform shear. *Dyn. Atmos. Ocean* **22**, 135–160.

Whitehead, J. A., Marshall, J. & Hufford, G. E. 1996 Localized convection in rotating stratified fluid. *J. Geophys. Res.* **101**, C10, 25 705–25 721.